Journal of Materials Science and Chemical Engineering, 2024, 12, 31-82
https://www.scirp.org/journal/msce
ISSN Online: 2327-6053
ISSN Print: 2327-6045

Research Progress of Solid Hydrogen Storage Materials for Hydrogen Energy Storage and Transportation

Xiaomei Zhu[1], Meijun Wang[2], Yongyan Xu[3], Zhiping Liu[1*], Yunfeng Si[1], Haijie Zhang[1], Wenbo Li[1]

[1]Department of Chemical Engineering, Ordos Institute of Technology, Ordos, China
[2]Sales Department, Baotou Tianjiao Seimi Polishing Powder Co. Ltd., Baotou, China
[3]Inner Mongolia Rare Earth Functional Materials Innovation Center Co. Ltd., Baotou, China
Email: *relzp@oit.edu.cn

How to cite this paper: Zhu, X.M., Wang, M.J., Xu, Y.Y., Liu, Z.P., Liu, Y., Li, W.B., Liu, Y.F., Si, Y.F. and Zhang, H.J. (2024) Research Progress of Solid Hydrogen Storage Materials for Hydrogen Energy Storage and Transportation. *Journal of Materials Science and Chemical Engineering*, **12**, 31-82.
https://doi.org/10.4236/msce.2024.1211004

Received: September 26, 2024
Accepted: November 25, 2024
Published: November 28, 2024

Abstract

With the rapid development of hydrogen energy, hydrogen storage alloys have attracted wide attention owing to their key advantages, such as high volume density, proper plateau pressure, environmental friendliness and good safety. In the present review, the research progress of the improvement in hydrogen storage alloys, including rare-earth-based alloys, Mg-based alloys, Ti/Zr-based alloys, V-based alloys and high entropy alloys are systematically summarized. The influences of elemental substitution, catalyst doping, preparation methods and nanotechnology on the crystal structure, hydrogen storage properties as well as their affecting mechanisms, are discussed. Furthermore, the development trend and future research directions are proposed, which are expected to bring novel research ideas and potentially applicable methods for the development of high-performance hydrogen storage alloys.

Keywords

Hydrogen Storage Alloy, Elemental Substitution, Preparation Method, Catalyst Doping, Nanotechnology

1. Introduction

Environmental pollution and energy crisis make it necessary for the development and utilization of clean energy. Hydrogen energy with the advantages of high energy density, nontoxicity, environmental friendliness and renewability, is playing an increasingly important role in the transportation, solar energy utilization, and fuel cell hybrid power generation [1], thus is regarded as an important part

of future energy development. Hydrogen industry chain includes hydrogen preparation, hydrogen storage and transportation, and hydrogen application, among which hydrogen storage and transportation is a key link between hydrogen production and hydrogen application, and therefore, remains a hot topic for years. There are three main hydrogen storage methods, which are high-pressure gaseous hydrogen storage, low-temperature liquid hydrogen storage and solid hydrogen storage. Among them, solid hydrogen storage has a good application prospect owing to its high-volume density, convenient transportation, and good safety [2]-[7]. Solid hydrogen storage materials include physical and chemical hydrogen storage materials [8]; Physical hydrogen storage materials mainly include activated carbon, activated carbon fibers, carbon nanofibers, carbon nanotubes and carbon aerogel, etc. [9]. chemical hydrogen storage materials mainly include metal hydride hydrogen storage materials, coordination hydride hydrogen storage materials and other hydrogen storage materials [10], metal hydride is the most mature at present [8]. The comparisons between different families of solid-state hydrogen storage materials are listed in **Table 1**. In physical hydrogen storage, hydrogen combines with materials in molecular form, and the force is very weak, basically van der Waals force [11]. Hydrogen storage capacity is related to the large surface area and porous structure of the material. At normal temperatures, the hydrogen storage capacity is relatively low, hydrogen absorption proceeds only at low temperatures (77 K or 87 K) [10], and the volume of hydrogen storage facilities is relatively large [12]. Chemical hydrogen storage refers to the use of metal hydrides and coordination hydrides as hydrogen storage materials. Metal hydride hydrogen storage materials store hydrogen in the form of metal hydrides [8]. To form reversible hydrides, it is necessary to combine element A, which forms strong hydrides, with element B, which forms weak hydrides, to create alloys (especially intermetallic compounds) that exhibit the desired thermodynamic properties [10]. These materials have a high hydrogen storage capacity at low pressures [12],

Table 1. Comparisons between different families of solid-state hydrogen storage materials.

	Materials	Mass hydrogen storage density (wt%)	Hydrogen storage mechanism	Hydrogen storage property
Physical hydrogen storage	Carbon-based hydrogen storage materials, inorganic porous materials	0.4 - 6.4 [8]	Van der Waals' force [11]	low hydrogen storage capacity [10], and large hydrogen storage facilities [12]
Chemical hydrogen storage	Metal hydride hydrogen storage materials	1.4 - 7.6 [8]	metal hydrides, (reversible hydrides) [10]	high hydrogen storage capacity, [12], stable metal or alloy materials, hydrogen absorption/desorption at higher temperature conditions [13]
	Coordination hydride hydrogen storage materials	~18 [10]	coordination complex [12]	high hydrogen storage capacity, poor reversible performance, produced harmful substances may be [13]

but the hydrides of metals or alloys are often too stable, resulting in hydrogen absorption and desorption occurring only under higher temperature conditions [13]. Coordination hydride hydrogen storage materials are complex hydrides formed by the covalent bond between hydrogen atoms and the central atom of the coordination complex [10] [12]. These materials have a high hydrogen storage capacity, but their reversible performance is poor, and harmful substances may be produced during the high-temperature dehydrogenation process [13].

At present, hydrogen storage alloys are the most applied and studied material for solid hydrogen storage because they usually have high volume density, proper plateau pressure, rapid hydrogen absorption/desorption and good safety. Meanwhile, they are also the only industrialized solid hydrogen storage material that can be used in the areas of hydrogen compression, thermal energy storage, electrochemical energy storage, etc. [8] [14].

Hydrogen storage alloys can absorb hydrogen to form metal hydrides at certain temperature and pressure conditions, and the reactions are usually reversible [15]. Hydrogen storage alloys are generally consisted of A-side elements that absorb hydrogen and B-side elements that basically do not absorb hydrogen but have catalytic effects. A-side elements are mainly metals in the IA-VB groups of the periodic table with high affinity with hydrogen, such as La, Ti, Zr, V, Mg, etc. They have a decisive influence on the hydrogen storage capacity. B-side elements are usually transitional metals such as Ni, Co, Mn, Al, Fe, Cu, Cr, etc., with low affinity with hydrogen, which mainly affect the formation of heat and the hydrogen absorption/desorption plateau pressure [16] [17]. According to the elemental composition, hydrogen storage alloys can be mainly divided into rare-earth-based (RE-based) hydrogen storage alloys, Mg-based hydrogen storage alloys, Ti-/Zr-based hydrogen storage alloys, V-based hydrogen storage alloys and high entropy alloys (HEAs) [18].

Mg_2Ni alloy is the earliest hydrogen storage alloy in history, and it was synthesized by Reilly *et al.* of Brookhaven National Laboratory in 1964 [19]. Since the late 1960s, $LaNi_5$, TiFe, Mg_2Ni and other intermetallic compounds with hydrogen storage ability were discovered by Philips Laboratory in Netherlands and Brookhaven National Laboratory in the United States. In 1984, Willims *et al.* obtained a $La_{0.8}Nd_{0.2}Ni_{2.5}Co_{2.4}Si_{0.1}$ alloy with long cycle life by partially substituting Co for Ni and slight Nd for La, which boosted the rapid development of hydrogen storage alloys [20]. In the early 1990s, rare-earth AB_5-type hydrogen storage alloys were industrialized owing to their rapid activation, good hydrogen absorption/desorption reversibility and stable cycling performance. With the maturation of the preparation technology and the decrease of material cost, hydrogen storage alloys realized the diversity in both products and applications. However, high-capacity hydrogen storage alloys usually have the problem of slow kinetics, while those with fast kinetics generally have low hydrogen storage capacity [21]. Therefore, the development of hydrogen storage alloys with good overall hydrogen storage properties of high capacity, easy activation, good thermodynamic and kinetics

properties, long cycle life and low cost has always been the research focus, and is also the key to realize the large-scale safe application of hydrogen energy. For the above purpose, domestic and foreign experts and scholars have carried out a lot of innovative works in aspects of elemental substitution, catalytic doping, preparation methods, surface modification, nanotechnology and so on [22]-[27].

The present review systematically summarizes the recent research progress in the development of hydrogen storage alloys, such as element substitution, catalytic doping, preparation methods and nanotechnology as well as their relationship to the hydrogen absorption/desorption mechanisms and properties of different types of hydrogen storage alloys, expecting to serves as a guide for the rational design of advanced hydrogen storage alloys with tailored elemental compositions and phase structures as well as improved overall hydrogen storage properties.

2. Rare-Earth-Based Hydrogen Storage Alloys

Rare-earth-based (RE-based) hydrogen storage alloys include AB_5-type alloys, La-Mg-Ni-based alloys and La-Y-Ni-based alloys. These alloys usually have good comprehensive hydrogen absorption/desorption performance [27]. Among RE-based alloys, AB_5-type alloys with advantages of fast activation, good reversibility and long cycle life are the earliest to realize industrialization, and are still one of the leading products in the market. The recent developed La-Mg-Ni-based and La-Y-Ni-based alloys have relatively higher hydrogen storage capacity than AB_5-type alloys. Moreover, they are also easily activated and have good high rate dischargeability (HRD) [28]. Attracted by their application potential, researchers have conducted extensive research on La-Mg-Ni-based and La-Y-Ni-based alloys in recent years.

2.1. RE-Based AB_5-Type Hydrogen Storage Alloys

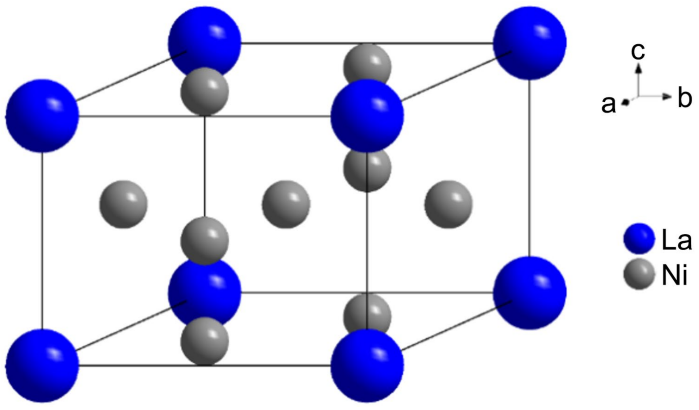

Figure 1. Crystal structure of $LaNi_5$ alloy.

For AB_5-type hydrogen storage alloys, the A-side elements are mainly rare-earth elements such as La, Ce, Pr, Nd, etc. and the B-side elements are mainly transitional metals such as Ni, Co, Mn, Al, Fe, Cu etc. The most basic AB_5-type

alloy is $LaNi_5$, the crystal structure of which is shown in **Figure 1**. Due to the limitation of the $CaCu_5$ lattice structure, the theoretical electrochemical hydrogen storage capacity of AB_5-type alloys is limited to 372 mAh·g^{-1} [29], and the actual discharge capacity is generally lower than 350 mAh·g^{-1}.

Elemental substitution is often applied to improve the electrochemical performance of AB_5-type hydrogen storage alloys. For example, for A-side elements, Fu *et al.* [23] partially substituted La for Ce in the $La_{1-x}Ce_xNi_{4.5}Al_{0.5}$ (x = 0 - 0.4) alloys to improve the hydrogen absorption/desorption thermodynamic properties. Results showed that the maximum hydrogen storage capacity (C_{max}) of the alloys decreased with the increase of Ce content. The absolute values of the enthalpy and entropy changes of the alloys first increased and then decreased. When x = 0.2, the absolute values of the enthalpy change for hydrogen absorption and desorption reached the lowest which were 26.33 kJ·mol^{-1} and 24.30 kJ·mol^{-1}, respectively. As Co is a high-cost element but indispensable to achieve good cycle life for AB_5-type alloys, many works have been carried out based on low-Co alloys. For example, Cheng *et al.* [30] partially substituted Y for Ce in the low-Co $La_{0.90-x}Ce_{0.08}Y_xZr_{0.02}Ni_{3.91}Co_{0.14}Mn_{0.25}Al_{0.30}$ (x = 0 - 0.7) alloys which led to the formation of the Ce_2Ni_7 secondary phase in the original $CaCu_5$ single-phase structure. Thus, the C_{max} and hydrogen diffusion of the alloys were improved, and the corrosion resistance was enhanced, but the pulverization resistance was reduced. The x = 0.3 alloy exhibited excellent electrochemical performance, with a C_{max} of 350.4 mAh·g^{-1}, a capacity retention rate after 100 cycles (S_{100}) of 80.15% and a HRD_{3000} of 73.56%. Kazakov *et al.* [31] studied three low-Co alloys $La_{0.8}Ce_{0.2}Ni_4Co_{0.4}Mn_{0.3}Al_{0.3}$ (La-alloy), $La_{0.6}Ce_{0.2}Nd_{0.2}Ni_4Co_{0.4}Mn_{0.3}Al_{0.3}$ (Nd-alloy) and $La_{0.6}Ce_{0.2}Nd_{0.2}Ni_{3.8}Co_{0.4}Mn_{0.3}Al_{0.3}Cr_{0.2}$ (Cr-alloy). It was found that the La-alloy had the highest hydrogen storage capacity and electrochemical discharge capacity, which were 1.23 wt% and 321.1 mAh·g^{-1}, respectively. The partial substitutions of Nd for La and Cr for Ni improved the cycle life of the alloy electrodes, but slightly reduced the C_{max}, *HRD* and hydrogen diffusion kinetics. After 100 charge/discharge cycles at 1C, the capacity retention of the Nd-alloy was as high as 92.2%.

For the modification of B-side elements, Han *et al.* [32] studied the effects of adjusting the content of Cu and Be elements simultaneously of the $La_{0.6}Ce_{0.2}Pr_{0.05}Nd_{0.15}Ni_{3.55}Co_{0.75-x}Mn_{0.4}Al_{0.3}$ $(Cu_{0.06}Be_{0.04})_x$ (x = 0 - 0.75) alloys. It was found that with the increase of Be-Cu content, the *HRD* of the alloys was improved, and the hydrogen storage capacity first increased and then decreased, with the peak value of 321.9 mAh·g^{-1} at x = 0.45. Zhou *et al.* [33] [34] studied the effects of partial substitution of Mn for Ni in $LaNi_{5-x}Mn_x$ and $La_{0.78}Ce_{0.22}Ni_{4.4-x}Co_{0.60}Mn_x$ alloys. Results showed that the discharge capacity and cycle stability of the alloys were slightly improved, but the equilibrium pressure was reduced, which had an adverse effect on low-temperature discharge capability and *HRD* performance. Xu *et al.* [35]. found that adding appropriate amount of Sn to $LaNi_5$ alloy could result in higher anisotropic *c/a* value, reducing the microstrain of the alloys and thus improving the cycle life. The S_{1000} of the $LaNi_{4.25}Sn_{0.75}$ alloy reached 95.8%. Zhou

et al. [36] believe that Al is a very important element for AB_5-type alloys and they showed that although Al-free AB_5-type hydrogen storage alloys may have higher surface catalytic capacity, better low-temperature and *HRD* performance, the cycle life would be poor. Comparisons between different B-side elements based on the $(LaCe)_{1.0}Ni_{3.8}(CoMn)_{1.05}Al_{0.05}M_{0.1}$ (M = Ni, Al, Fe, Si, Sn, Cu) alloys showed that larger atomic radius led to higher hydrogen storage capacity and hydride thermodynamic stability, but was not favorable for low-temperature performance. The low-temperature discharge ability, *HRD* and peak power gradually decreased in the order of Ni > Si > Fe > Sn > Cu > Al, but the cycling stability was increased. The $(LaCe)_{1.0}(NiCoMn)_{4.85}Al_{0.05}Cu_{0.1}$ alloy exhibited the best overall electrochemical properties.

Stoichiometry modification is also applied to optimize the elemental composition of AB_5-type alloys. Chen *et al.* [37] studied the effects of over-stoichiometry based on a series of $La_{0.582}Ce_{0.191}Zr_{0.025}Sm_{0.202}(Ni_{0.849}Co_{0.032}Mn_{0.05}Al_{0.069})_{5+x}$ (x = 0 - 0.47) alloys and found that over-stoichiometry was beneficial to the cycle stability. The x = 0.35 alloy displayed a high S_{100} of 96.71% enabled by the enhanced anti-pulverization resistance and weakened electrode polarization.

The characteristics of elemental compositions can be useful in the prediction of hydride thermodynamic properties. Prompted by the requirement of fast design of novel AB_5-type hydrogen storage alloys for industrialization, Panwar *et al.* [38] established a structural model of the correlation between the thermodynamic properties and structural parameters of the multi-element AB_5-type alloys. The model connects the atomic radius of the elements with the heat of formation to calculate the "hydride formation enthalpy" of the binary, ternary and multicomponent AB_5-type metal hydrides.

Different treatments such as rapid solidification, annealing etc. have also been used to improve the hydrogen storage properties of AB_5-type alloys. Yao *et al.* [39] studied the effects of rapid solidification on the structure and hydrogen storage performance of the $LaNi_{4.5}Co_{0.25}Al_{0.25}$ alloy. It was found that rapid solidification could improve the uniformity of the constituent elements and expand the crystal lattices, thus improving the activation properties, cycle stability and self-discharge performance, but the *HRD* was jeopardized. Zhu *et al.* and Kazakov *et al.* [40] [41] studied the effects of annealing and found that annealing usually do not change the $CaCu_5$-phase structure of AB_5-type alloys, but could improve the cycling stability. For example, the cycle life of the $MlNi_{4.57}Co_{0.17}Mn_{0.25}Al_{0.41}Y_{0.02}$ and $La_{0.8}Ce_{0.2}Ni_4Co_{0.4}Mn_{0.3}Al_{0.3}$ alloys was improved significantly prolonged by annealing. However, with the increase of eighter annealing temperature or holding time, the C_{max} and the *HRD* performance were decreased, and the impact of annealing temperature was stronger than that of annealing time.

Surface treatment improves the surface characteristics which ameliorate the hydrogen storage properties of AB_5-type alloys. Gan *et al.* [42] modified the surface of the $MlNi_{4.07}Co_{0.45}Mn_{0.38}Al_{0.31}$ alloy using the mixed solution of 12 mol·L^{-1} NaOH + 0.5 mol·L^{-1} NH_4F + 0.1 mol·L^{-1} KBH_4. After the modification, nano sticks were

formed on the alloy surface. Al, Mn and Fe elements were partially dissolved, forming a Ni-rich surface layer. Resultantly, The *HRD* performance of the alloy was improved with a specific capacity of 120.6 $mAh \cdot g^{-1}$ at the discharge current density of as high as 10 C. Hubkowska *et al.* [43] synthesized Pd nanoparticles of irregular shape and size on the surface of $LaMmNi_{4.1}Al_{0.3}Mn_{0.4}Co_{0.45}$ alloy by using microwave assisted polyol method which not only enhanced the hydrogen absorption/desorption kinetics performance but also spared the electrochemical activation process.

In addition, the degradation mechanism has also been explored to improve the cycle life of AB5-type hydrogen storage alloys. For example, Zhu *et al.* [44] studied the degradation progress of the AB_5-type $LaNi_{4.75}Mn_{0.25}$ alloys based on the structure and hydrogen absorption/desorption data during long-term cycling. It was found that in the temperature range of 343 - 383 K, the PCT curves of the alloys remained a single plateau within 1000 cycles, but the slope of the plateau became steeper and the hydrogen storage capacity decreased. Further study revealed that the degradation phenomenon was caused by the structural evolution, including pulverization and lattice damage. The internal driving force of the structural change was the microstrain generated during hydrogen absorption/desorption. However, the isotropic parameter *c/a* increased with cycling, reducing the hysteresis and slowing down the degradation process.

2.2. RE-Mg-Ni-Based Hydrogen Storage Alloys

RE-Mg-Ni-based hydrogen storage alloys have super-stacking structures consisting of $[A_2B_4]$ and $[AB_5]$ subunits stacking along *c*-axis. The most common RE-Mg-Ni-based alloys are La-Mg-Ni-based alloys and the ratios between $[A_2B_4]$ and $[AB_5]$ subunits mainly include 1:1, 1:2 and 1:3, which correspond to $(La, Mg)Ni_3$, $(La, Mg)_2Ni_7$ and $(La, Mg)_5Ni_{19}$ phases, respectively. Each of these phases has two crystal types: hexagonal (2H-) type and rhombohedra (3R-) type. The typical superstacking modes are presented in **Figure 2**. RE-Mg-Ni-based alloys have the advantages of both high capacity of AB_2-type alloys and easy activation and fast hydrogen absorption/desorption rate of AB_5-type alloys [28]. However, the overall hydrogen storage properties especially cycle life still need to be further improved for practical applications [45]. The cyclic degradation mechanism of RE-Mg-Ni-based alloys was explored based on a $LaSmMgNi_{4.1}$ alloy composed of $(LaSm)MgNi_4$ and $LaNi_5$ phases [46]. It was found that after absorption/desorbing cycling, the $(LaSm)MgNi_4$ main phase decomposed from crystalline state to (LaSm) hydride and MgNi-H amorphous state. Moreover, progressive cracking and pulverization of the alloy particles also led to the cycling degradation. To relieve the capacity degradation during cycling, extensive works have been carried out.

Mg is found to be a very important element for stabilizing the structure of RE-Mg-Ni based alloys. Chen *et al.* [47] have reported that the $La_{3-x}Mg_xNi_9$ alloys are mainly formed from the bond interactions between La-Ni, Ni-Ni or/and M-Ni, and La-Ni which is the main factor controlling the structural stability of the alloys. Mg substitution for La could enhance the interaction of the La-Ni bond which

increases the cycling stability of the alloys. However, high Mg content would also lead to the reduction of cell volume and decrease the hydrogen storage capacity. Wang *et al.* [48] found that appropriate amount of Mg could promote the formation of Gd_2Co_7 and Ce_2Ni_7 main phases of the $La_{1-x}Mg_xNi_{3.4}Al_{0.1}$ (x = 0.1 - 0.4) alloys. The alloy with x = 0.2 showed good electrochemical performance with the C_{max} of 357.4 mAh·g^{-1}, HRD_{1200} of 60.1% and S_{100} of 74.5%. Moreover, the fine $LaNi_5$ structure dispersed in the $(La,Mg)_2Ni_7$ matrix phase could promote the diffusion of hydrogen atoms, thus enhancing the electrochemical properties of the alloys. Dong *et al.* [49] prepared a series of single-phase $La_{1-x}Mg_xNi_{2.5}Co_{0.5}$ (x = 0 - 0.4) alloys with $PuNi_3$-type phase structure by annealing and studied the effects of Mg content. It was found that with hydrogen absorption, the hydrides gradually transformed from amorphous state to $PuNi_3$-type crystal, and the lattice parameters a and c significantly increased, leading to the expansion of cell volume. But the expansion degree decreased with the increase of Mg content which benefits the cycling stability of the alloys.

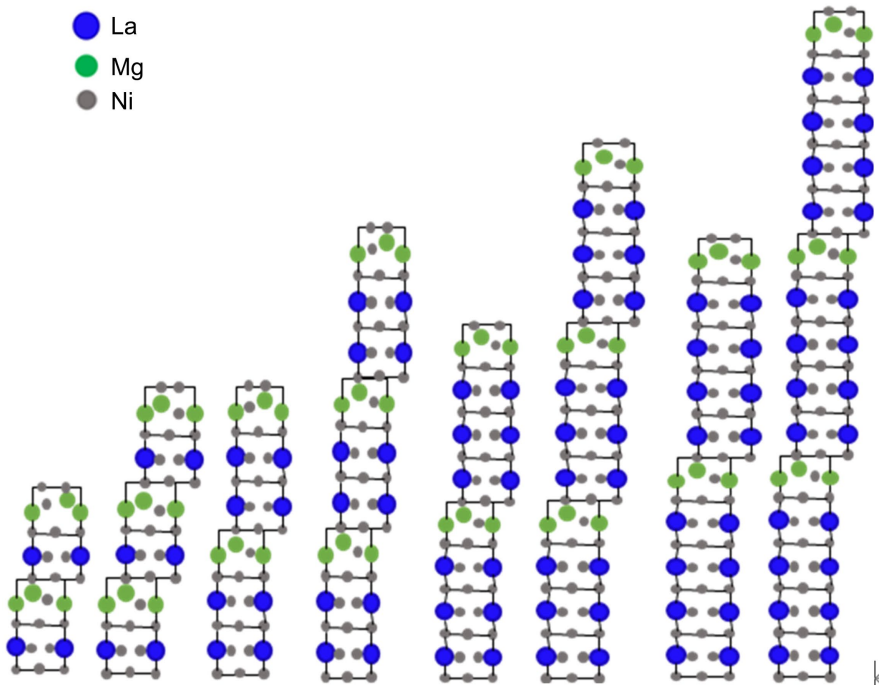

Figure 2. Stacking modes of AB_3-, A_2B_7-, and A_5B_{19}-type La-Mg-Ni-based alloys.

In addition to Mg, the effects of other A-side elements have also been studied. For example, Zhou *et al.* [50] partially substituted La with mixed rare earth (MM) for the $La_{0.8-x}MM_xMg_{0.2}Ni_{3.1}Co_{0.3}Al_{0.1}$ (x = 0 - 0.3) alloys, and found that the addition of MM could lead to more uniform phase distribution and promote the formation of the La_2Ni_7 phase with good electrochemical properties. The alloy with x = 0.3 achieved the C_{max} of 381.2 mAh·g^{-1} and HRD_{1500} of 60.55%. Xu *et al.* [51] found that the addition of Ce in the $La_{0.8-x}Ce_xMg_{0.2}Ni_{3.8}$ (x = 0 - 0.5) alloys promoted the formation of the A_5B_{19} phase. The activation property, capacity

retention and *HRD* of alloy electrodes were all enhanced with the increase of Ce content, and the S_{100} reached 86.17% when $x = 0.5$. Huang *et al.* [52] studied the effects of Pr substitution for La of the $La_{0.7-x}Pr_xZr_{0.1}Mg_{0.2}Ni_{2.75}Co_{0.45}Fe_{0.1}Al_{0.2}$ ($x = 0$ - 0.20) alloys and found that the anti-corrosion effect of Pr enabled the enhancement of the alloys' cycling stability which S_{200} reached 75.1% for the $x = 0.2$ alloy. But the cell parameters of the alloy phases decreased, which hindered the diffusion of hydrogen atoms, decreasing the dynamics property. Liu *et al.* [53] proposed a new strategy to improve the cyclic stability of superlattice hydrogen storage alloys by enhancing the structural stability and oxidation/corrosion resistance by A-side elemental modification. Specifically, they equalized the volumes of [$LaMgNi_4$] and [$LaNi_5$] subunits taking the advantages of site occupation tendency of Gd in the $La_{0.75-x}Gd_xMg_{0.25}Ni_{3.5}$ ($x = 0$ - 0.15) alloys, so as to maintain a stable crystal structure during cycling. In addition, the high electronegativity of Gd element enhanced the oxidation/corrosion resistance of the alloys and the S_{100} of the $x = 0.15$ alloy reached 88.2%.

For B-side elements, Li *et al.* [54] studied the effects of partial substitution of Zn for Ni in the $La_2Mg(Ni_{1-x}Zn_x)_9$ ($x = 0.1$ - 0.2) alloys, and found that appropriate amount of Zn could significantly improve the cycle stability of the alloys due to the formation of the dense passivation film on the alloy surface. The S_{100} of the $La_2Mg(Ni_{0.9}\ Zn_{0.1})_9$ alloy reached as high as 94%. Wang *et al.* [55] reported that the Al-substituted $La_{0.60}Nd_{0.15}Mg_{0.25}Ni_{3.20}Al_{0.10}$ alloy exhibited good cycle stability, and the Mn-substituted $La_{0.60}Nd_{0.15}Mg_{0.25}Ni_{3.20}Mn_{0.10}$ alloy was with increased discharge capacity, reduced plateau pressure and enhanced *HRD* performance. Moreover, Fan *et al.* [56] studied the influence of non-stoichiometric ratio on the phase composition and electrochemical properties of the of the A_5B_{19}-A_2B_7 double-phase La_4MgNi_x ($x = 16$, 17, 18) alloys and found that the increase of x value contributed to the formation of A_5B_{19} phase and the $x = 17$ alloy was with the highest discharge capacity (388.8 $mAh{\cdot}g^{-1}$) and the best cycle life ($S_{100} = 90.1\%$).

Doping of elements is also companied by the change of elemental composition, but the alloys' properties are also influenced by the doping method. For example, Zhang *et al.* [57] doped pure Ni to the LaMgNi alloy by ball milling which not only promoted the amorphization process of the alloy particles but also enhanced the catalytic effect. The hydrogen absorption/desorption kinetics of the Ni-doped LaMgNi + wt%Ni ($x = 100$, 200) alloys was significantly improved. With increasing ball milling time, the gaseous hydrogen absorption capacity and kinetics of the alloys first increased and then decreased, but the hydrogen desorption kinetics was always increased. Further studies showed that both increasing nickel content and prolonging the ball milling time could significantly reduce the activation energy of the alloy for hydrogen desorption. Zhang *et al.* [58] synthesized a Y_2O_3@$La_{1.7}Mg_{1.3}Ni_9$ composite by ball milling, and found that Y_2O_3 was coated on the alloy surface which was mostly in amorphous state. The modified alloy exhibited better corrosion resistance, electrochemical hydrogen storage capacity, and cycling stability.

Treatment methods such as rapid quenching and annealing have also been widely investigated to improve the hydrogen storage properties of RE-Mg-Ni-based alloys. For example, Hu *et al.* and Luo *et al.* [21] [59] compared the as-cast alloy and those after rapid quenching. Results showed that the as-cast alloy was composed of multiphase structure, while those after rapid quenching contained a large number of amorphous nanocrystalline structure whose content increased with the increase of solidification rate. Rapid quenching could reduce the activation energy of the alloy surface and enhance the diffusion ability of hydrogen atoms, so as to improve the electrochemical kinetics performance of the alloys. Li *et al.* [60] studied the microstructure evolution of the $La_{2-x}Mg_xNi_7$ ($x = 0.3, 0.4$) alloys after annealing treatment and found that the characters of the annealed microstructure originated from that of the as-cast microstructure, indicating the heredity effect between the as-cast and annealed microstructure. Moreover, the abundance of the $(La, Mg)_2Ni_7$ main phase increased in sacrifice of the $(La, Mg)Ni_2$ and $LaNi_5$ phases after annealing. Chen *et al.* [61] reported that annealing unified the elemental distribution of the $LaMgNi_{3.9}Mn_{0.2}$ alloy whose structure was mainly columnar crystal. They also found heredity effect for the annealed alloy from the as-cast one. Moreover, with the increase of annealing time, the $LaMg(NiMn)_4$ phase content decreased and the $(La, Mg)(NiMn)_5$ phase content increased. Deng *et al.* [62] demonstrated that annealing treatment improved the cycling stability of the $(Pr_{0.1}Nd_{0.1}Y_{0.6}Sm_{0.1}Gd_{0.1})_{0.2}Mg_{0.17}Ni_{3.1}Co_{0.3}Al_{0.1}$ alloy and the S_{100} increased from 69% of the as-cast alloy to 83.5% of the annealed alloy. Moreover, they also found that the controlling factor of the *HRD* altered from hydrogen diffusion to surface charge transfer. Jiao *et al.* [63] found that annealing could eliminate the AB_5 secondary phase and increase the total content of superlattice phases in the $La_{0.75}Mg_{0.25}Ni_{3.5}$ alloy, thus improving the discharge capacity. Meanwhile, the homogenization and stress reduction of the $(La, Mg)_2Ni_7$ and $(La, Mg)_5Ni_{19}$ superlattice phases of the annealed alloy could relive the pulverization and oxidation of the alloy particles during charge/discharge cycling, and significantly improve the cycling stability of the alloy electrodes. The C_{max} of $La_{0.75}Mg_{0.25}Ni_{3.5}$ alloy electrode was 367 $mAh \cdot g^{-1}$, and the S_{100} was 81.47%. However, due to the decrease of defects and grain boundaries, the *HRD* performance of the alloy was decreased. Similarly, Young *et al.* [64] also reported that annealing increased the abundance of the A_2B_7 main phase and decreased the that of the AB_5 secondary phase of the $(Nd_{0.87}Mg_{0.12}Zr_{0.01})(Ni_{0.952}Al_{0.046}Co_{0.002})_{3.74}$ alloy. Moreover, the cell volume of the main phase became smaller, and the elemental distribution became more uniform. Both the hydrogen storage capacity and the electrochemical discharge capacity of the alloy were improved by annealing, and the slope factor and the hysteresis were also reduced which enhanced the activation, *HRD*, and cycle life of the alloy. They also found that with the increase of annealing temperature, the AB_5 phase abundance decreased, which further improved the hydrogen storage capacity and cycle life of the alloy. Increasing the annealing time led to the increase of the A_2B_7 phase abundance, which improved the discharge capacity and

cycle life of the alloy, but the *HRD* was reduced due to the decrease of AB_5 catalytic phase.

2.3. La-Y-Ni-Based Hydrogen Storage Alloys

La-Y-Ni-based hydrogen storage alloys have similar super-stacking structures to La-Mg-Ni-based alloys. The stoichiometries of this alloy system include AB_3-type, A_2B_7-type and A_5B_{19}-type. The preparation process of La-Y-Ni-based alloys is simpler than that of La-Mg-Ni-based alloys enabled by the possible exclusion of Mg element with high vapor pressure. He *et al.* [65] studied the phase transition process and hydrogen storage properties of different types of La-Y-Ni-based alloys with various $[AB_5]/[A_2B_4]$ ratios. They reported that the transformation process could be summarized as $A_2B_4 + AB_5 \rightarrow AB_3 \rightarrow A_2B_7 \rightarrow A_5B_{19}$. Usually, with the increase of the $[AB_5]/[A_2B_4]$ ratio, the hydrogen absorption plateau pressure increases ($LaY_2Ni_9 < La_2Y_4Ni_{21} < La_5Y_{10}Ni_{57}$), the stability of the corresponding hydrides decreases, the maximum discharge capacity decreases, and the cycling stability increases. Among the LaY_2Ni_9, $La_2Y_4Ni_{21}$ and $La_5Y_{10}Ni_{57}$ alloys, the $La_2Y_4Ni_{21}$ alloy exhibited the best *HRD* performance, and the solid hydrogen storage capacity was also high (1.59 wt% at 313 K). Yan *et al.* [66] also compared different types of $LaY_2Ni_{8.2}Mn_{0.5}Al_{0.3}$ (AB_3), $LaY_2Ni_{9.7}Mn_{0.5}Al_{0.3}$ (A_2B_7) and $LaY_2Ni_{10.6}Mn_{0.5}A1_{0.3}$ (A_5B_{19}) alloys and found that under the same temperature, the alloys' plateau pressure was in the order of $A_5B_{19} > A_2B_7 > AB_3$. The highest hydrogen storage capacity was obtained for the AB_3-type $LaY_2Ni_{9.7}Mn_{0.5}Al_{0.3}$ alloy which was 1.48 wt% at 313K, and the maximum discharge capacity of the alloy electrode was 385.7 $mAh{\cdot}g^{-1}$. All the three alloys showed good cycling stability. The S_{300} was above 74%, but the *HRD* performance was lower than that of AB_5-type alloys.

Elemental composition has significant influence on the structure and hydrogen storage properties of La-Y-Ni-based alloys. Y for La-Y-Ni-based alloys resembles Mg for La-Mg-Ni-based alloys and the amount of Y can have great impact on the comprehensive electrochemical performance. Zhao *et al.* [67] found that the main phase of $La_{1-x}Y_xNi_{3.25}Mn_{0.15}Al_{0.1}$ (x = 0 - 1) alloy was of Ce_2Ni_7 phase. With the increase of Y content, the Ce_2Ni_7 phase abundance first increased and then decreased. Moreover, the higher the Ce_2Ni_7 phase abundance was, the higher the HRD_{900} value was. When x = 0 - 0.25, the alloys had no plateau in the PCT curves and were easy to become amorphous during hydrogen absorption/desorption. When $x \geq 0.50$, hydrogen-induced amorphization was effectively inhibited and a single hydrogen absorption/discharge plateau was obtained. The pressure range of the hydrogen absorption plateau was 0.026 - 0.097 MPa, and the maximum hydrogen storage capacity was 1.418 - 1.48 wt%. Liu *et al.* [68] found that the capacity and *HRD* performance of the $La_{3-x}Y_xNi_{9.7}Mn_{0.5}Al_{0.3}$ (x = 1 - 2.5) alloys also increased with the increase of Y content. The highest C_{max} and HRD_{1200} reached 383.8 $mAh{\cdot}g^{-1}$ and 83.67%, respectively at x = 2.5. Guo *et al.* [69] compared the effect of Y and Mg in the AB_3-type $LaY_{2-x}Mg_xNi_9$ (x = 0 - 1.00) La-Y-Ni-based alloys, and found that the addition of Mg decreased the LaY_2Ni_9 phase abundance

while increased the $(La, Y)_2Ni_7$ phase abundance, which improved the alloys' cycling stability by slowing down pulverization, but reduced the maximum discharge capacity. TEM results further verified that Mg substitution could inhibit the hydrogen-induced amorphization, benefiting the cycling stability of the alloys. The $LaY_{1.25}Mg_{0.75}Ni_9$ alloy showed good overall electrochemical performance with the C_{max} of 308.4 mAh·g^{-1} and S_{100} of 93.7%.

The effects of A-side rare-earth elements have also been widely studied for La-Y-Ni-based alloys. Zhao *et al.* [70] reported that the addition of Nd in the La-Y-Ni-based $La_{0.4-x}Nd_xY_{0.6}Ni_{3.52}Mn_{0.18}Al_{0.1}$ (x = 0 - 0.4) alloys could improve the cycling stability and *HRD* performance. Nd enables the formation of small and dense rare-earth oxide on the alloy surface which inhibits the dissolution of active materials such as Y, Mn and Al, and thus significantly improves the cycling stability of the alloy electrodes. The x = 0.4 alloy showed the best electrochemical performance with the C_{max} of 382.8 mAh·g^{-1}, S_{100} of 93.7%, and HRD_{900} of 87.8%. By comparing the $LaSm_{0.3}Y_{1.7}Ni_{9.7}Mn_{0.5}Al_{0.3}$ and $LaY_2Ni_{9.7}Mn_{0.5}Al_{0.3}$ alloys, Guo *et al.* [71] found that partial substitution of Sm for Y could enhance the corrosion resistance and anti-pulverization ability of the alloys, resulting in the improvement of cycle life. Yang *et al.* [72] compared the microstructure and electrochemical properties of the $La_{0.63}X_{0.2}Mg_{0.17}Ni_{3.1}Co_{0.3}Al_{0.1}$ (x = Pr, Nd, Y, Sm and Gd) alloys. It was found that the x = Y alloy contained the highest amount of Ce_2Ni_7 phase (93.3 wt%) and superior electrochemical discharge capacity (404.4 mAh·g^{-1}) and capacity retention (S_{100} = 93.50%).

For the effects of B-side elements on the structure and hydrogen storage properties of La-Y-Ni-based alloys, Al and Mn are the mostly studied. For example, Li *et al.* [73] found that Al addition could improve the cycle life of the $LaY_{1.9}Ni_{10.2-x}Al_xMn_{0.5}$ (x = 0 - 0.6) alloys but the function was limited as Al could not inhibit the pulverization of the alloy powder. Xiong *et al.* [74] found that partial substitution of Mn for Ni in the $LaY_2Ni_{10.5-x}Mn_x$ (x = 0 - 2.0) alloys increased the Ce_2Ni_7 phase abundance and expanded the cell volumes of the main phases, leading to the decrease in the hydrogen absorption/desorption equilibrium pressure. The C_{max} and *HRD* first increased and then decreased, and the x = 0.5 alloy exhibited the highest hydrogen storage capacity of 1.40 wt% with the corresponding discharge capacity of 392.9 mAh·g^{-1}. However, Yu *et al.* found that the increase of Mn content of the $La_{5.42}Y_{18.50}Ni_{76.08-x}Mn_x$ (x = 0 - 6) alloys reduced the Y_2Ni_7 and La_2Ni_7 phase contents while increased the LaY_2Ni_9 phase abundance, inhibiting the hydrogen induced amorphization and increasing the C_{max} of the alloys. Zhou *et al.* [75] found that with the increase of Mn content, the Ce_2Ni_7 phase abundance of the $La_{1.3}Ce_{0.5}Y_{4.2}Ni_{20-x}Mn_xAl$ (x = 0 - 0.7) alloys increased, leading to the increase of C_{max}. However, the decrease of the Gd_2Co_7 phase resulted in the decrease of the low-temperature discharge capacity from 286.6 mAh·g^{-1} (x = 0) to 64.7 mAh·g^{-1} (x = 0.7) at −30˚C. In addition, with the increase of Mn content, the kinetics performance of the alloys was also decreased significantly.

Annealing treatment is a very effective method to optimize the hydrogen

storage performance of La-Y-Ni-based alloys and thus has been widely studied. It is generally recognized that long-time annealing promotes microstructure homogenization, increases the main phase abundance, and thus improves the alloys' hydrogen storage performance [76]-[80]. For example, Wang *et al.* found that annealing increased the content of the Ce_2Ni_7 main phase of the $La_{0.33}Y_{0.67}Ni_{3.25}Mn_{0.15}Al_{0.1}$ alloy [76]. Li *et al.* [77] found that annealing the $La_{0.4}Y_{0.6}Ni_{3.52}Mn_{0.18}Al_{0.1}$ alloy at 1173 - 1373 K increased the Ce_5Co_{19} phase abundance which improved the discharge capacity, *HRD* performance and cycling stability of the alloy electrode. When the annealing temperature was 1273 K, the phase abundance of the Ce_5Co_{19} phase reached the highest so as the electrochemical performance of the alloy. Guo *et al.* [78] found that with the increase of annealing temperature (1073 - 1373 K), the C_{max}, *HRD* performance and cycling stability of the $LaY_2Ni_{9.7}Mn_{0.5}Al_{0.3}$ alloy electrode first increased and then decreased which was consistent with that of the main Ce_2Ni_7 phase abundance. Li *et al.* [79] found that as the annealing temperature increased from 1173 K to 1373 K, the Ce_5Co_{19} phase abundance of the $La_{0.35}Y_{0.65}Ni_{3.5}Mn_{0.2}Al_{0.1}$ alloy first increased and then decreased. The HRD_{900} and D_0 also showed a positive correlation with the Ce_5Co_{19} phase abundance. Moreover, when the annealing temperature was 1273 K, the corrosion current density was the least, and the cycle stability was the best. Zhou *et al.* [80] found that with the increase of annealing temperature (1098 - 1323 K), the low temperature performance of the $La_{1.9}Y_{4.1}Ni_{20.8}Mn_{0.2}Al$ alloy first increased and then decreased. At the annealing temperature of 1148 K, the alloy obtained modified H_2 channel, high dehydrogenation plateau pressure, good oxidation/corrosion resistance and good kinetics characteristics. The C_{max} at low temperature (243 K) was 298.6 mAh·g^{-1}, and the S_{100} reached 80.5%.

Through long-time annealing at appropriate temperatures, single-phase La-Y-Ni-based alloys could be obtained. Zhao *et al.* [81] prepared a single-phase $LaY_2Ni_{10.5}$ alloy with a rhombohedral Gd_2Co_7 structure by annealing at 1000˚C and a hexagonal Ce_2Ni_7 structure by annealing at 1100˚C. A double Gd_2Co_7-Ce_2Ni_7 phase structure was obtained when the temperature was between 1000˚C and 1100˚C. In other words, the rhombohedral structure is more stable than the hexagonal structure at low temperature. Based on the single-phase alloys, further study was carried out which showed that Y atom preferentially replaces La in the $[A_2B_4]$ subunit of the hexagonal and rhombohedral superlattice structures. Compared with the rhombohedral phase, the hexagonal phase has a relatively small $[A_2B_4]$ subunit volume, and thus showed higher structural stability during the hydrogen absorption/desorption cycling. Compared with multiphase alloys, single-phase alloys displayed better capacity, rate performance and cycle stability. The same group also obtained a single-phase $La_{0.33}Y_{0.67}Ni_{3.25}Mn_{0.15}Al_{0.1}$ alloy with a 2H-Pr_5Co_{19} structure by annealing the alloy at 1100˚C [82]. They reported that Y preferentially occupies the $[A_2B_4]$ subunit, Mn preferentially occupies the $[AB_5]$ subunit, and Al locates at the boundaries between $[A_2B_4]$ and $[AB_5]$ subunits. Reduced volume mismatch between $[AB_5]$-1, $[AB_5]$-2 and $[A_2B_4]$ subunits could improve

the electrochemical performance of the alloys. The C_{max} was 368.8 mAh·g^{-1}, the S_{200} was 73.4%, and the HRD_{1500} was 58.6% for the single-phase $La_{0.33}Y_{0.67}Ni_{3.25}Mn_{0.15}Al_{0.1}$ alloy. Xing *et al.* [83] compared the alloy treated with annealing with rapid quenching, and found that annealing treatment improved the C_{max} and *HRD* performance, while decreased the gaseous hydrogen absorption/desorption cycling stability. The rapid quenched alloy exhibited excellent cycling stability due to its good anti-pulverization resistance. After 30 cycles of gaseous hydrogen absorption/desorption, the particle size retention rate the rapid quenched La_4MgNi_{19} alloy reached 98.6%.

Moreover, considering that carbon has good electrocatalytic activity, electrical conductivity and corrosion resistance, Wu *et al.* [84] coated the (LaSmY) $(NiMnAl)_{3.5}$ alloy with different contents (0.1 wt% - 1.0 wt%) of nano-carbons by low-temperature sintering with sucrose as the carbon source. Results showed that the C_{max}, *HRD* and cycle stability of the alloy electrodes first increased and then decreased with the increase of carbon content. The electrochemical performance of the alloy electrode with carbon content of 0.3 wt% was the best with the C_{max} of 359.0 mAh·g^{-1}, the S_{300} of 80.01%, and the HRD_{1200} of 74.39%. The kinetics results showed that carbon coating could improve the electrocatalytic activity and conductivity of the alloy electrodes

3. Mg-Based Hydrogen Storage Alloys

Typical representatives of Mg-based hydrogen storage alloys include Mg metal and Mg_2Ni alloy whose crystal structures are presented in **Figure 3(a)**, **Figure 3(b)**. Mg-based alloys have abundant resources, low price, low density and high hydrogen storage capacity. The theoretical hydrogen storage capacity of MgH_2 is as high as 7.6 wt%. But the slow hydrogen absorption/desorption kinetics, poor thermodynamic properties (the heat formation of MgH_2 is up to −74.5 kJ·mol^{-1}, and the hydrogen desorption temperature is above 300˚C), large kinetics hysteresis and poor corrosion resistance have been limiting their practical applications [18] [20] [28] [85]-[87].

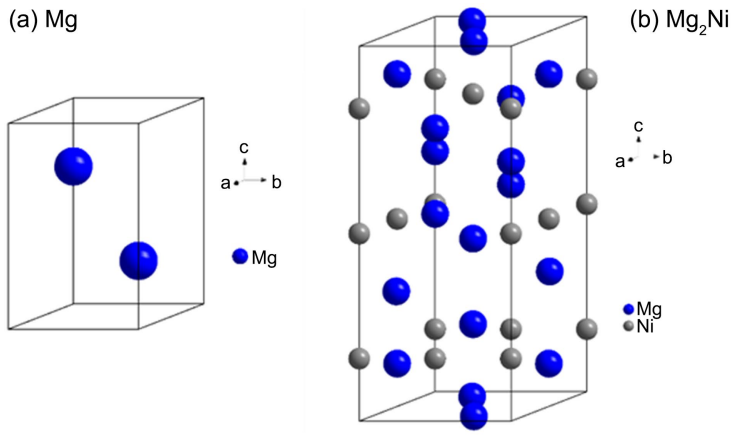

Figure 3. Crystal structure of Mg metal (a) and Mg_2Ni alloy (b).

The additions of rare-earth elements and transitional metals can effectively improve the thermodynamic stability of Mg-based hydrides and thus enhance their hydrogen absorption/desorption kinetics properties. Li *et al.* [88] found that the addition of Y could significantly improve the hydrogen absorption kinetics of the $Mg_{80-x}Ni_{20}Y_x$ (x = 0 - 7) alloys, and the entropy and enthalpy changes of the formation and decomposition of MgH_2 and Mg_2NiH_4 decreased with the increase of Y content. But the irreversible hydrogen storage capacity decreased due to the formation of YH_2. Zhang *et al.* [89] found that partial substitution of La by Y in the $La_{2-x}Y_xMg_{16}Ni$ (x = 0 - 0.4) alloys refined the alloys' structure and many nanocrystal grains were produced during hydrogen absorption/desorption, which resulted in many grain boundaries that provided hydrogen diffusion paths and active sites for hydrogen absorption/desorption reactions. Meanwhile, the partial substitution of Y for La weakened the Mg-H bond, leading to the decrease of the thermal stability of the alloys, which greatly improved the dehydrogenation kinetics, enhanced the activation properties, and accelerated the hydrogen absorption/desorption rate. The dehydrogenation activation energy of the alloys decreased from 84.5 kJ·mol^{-1} (x = 0) to 77.2 kJ·mol^{-1} (x = 0.4). Gao *et al.* [90] found that the addition of La in the $(Mg_{24}Ni_{10}Cu_2)_{100-x}La_x$ (x = 0 - 20) alloys induced the secondary La_2Mg_{17} and $LaMg_3$ phases to the Mg_2Ni main phase and produced nanocrystalline-amorphous structure in the alloys, which reduced the activation energy of hydrogen desorption, and thus improved the hydrogen desorption kinetics. Kang *et al.* [91] prepared $Mg_{90}Ce_{10}$, $Mg_{90}Ce_5Ni_5$ and $Mg_{90}Ce_3Ni_4Y_3$ alloys to study the effect of Ce, Ni, and Y elements on the hydrogen storage behavior of Mg-based alloys with fixed Mg content. Results showed that the reaction mechanism of the $Mg_{90}Ce_{10}$ alloy is a reversible cycling of Mg/MgH_2 catalyzed by $CeH_{2.73}$ phase. The addition of Ni element played a very important role in improving the hydrogen absorption/desorption kinetics of the Mg-Ce alloy. The optimum hydrogenation temperature of the alloy was optimized to 250˚C and the dehydrogenation activation energy was reduced from 127.3 k kJ·mol^{-1} ($Mg_{90}Ce_{10}$) to 79.7 kJ·mol^{-1} ($Mg_{90}Ce_5Ni_5$). After further addition of Y, the hydrogen absorption kinetics of the alloy was significantly enhanced and the hydrogen absorption capacity of the $Mg_{90}Ce_3Ni_4Y_3$ alloy alomst reached the maximum hydrogen absorption capacity (5.8 wt%) within 5 min. Yong *et al.* [92] found that the $Mg_{90}(Ce, Y)_{10-x}Ni_x$ (x = 1 - 9) alloys mainly consisted of $REMg_x$, Mg_2Ni and Mg phases. After hydrogenation, the REH_x phase was more favorable for hydrogen absorption and the Mg_2NiH_4 phase was more favorable for hydrogen desorption. The alloys exhibited excellent kinetics properties under the synergetic catalytic effects of Mg_2Ni/Mg_2NiH_4 and $(Ce,Y)H_2$. The x = 5 alloy displayed the best comprehensive hydrogen storage performance with a hydrogen absorption capacity of 5 wt% within 2 min and a desorption time of 10 min at 300˚C. Further kinetics study showed that with the increase of Ni content, the rate limiting step of the hydrogen desorption process changed from a surface control process to a random nucleation and growth process, resulting in a decrease in activation energy. Hao *et al.*

[93] prepared a Mg_2Ni-type $Mg_{22}Y_2Ni_{10}Cu_2$ alloy with Y and Cu partially substituting for Mg and Ni, respectively which has a typical lamellar eutectic organization structure with the phase composition of Mg_2Ni, $YMgNi_4$ and a small amount of Mg. Among these phases, no amorphization was observed after several hydrogen absorption/desorption cycles, indicating high structural stability. The additions of Y and Cu exhibited a certain catalytic effect on the hydrogen absorption properties of the Mg_2Ni-type alloys. The hydrogenation enthalpy change and entropy change of the $Mg_{22}Y_2Ni_{10}Cu_2$ alloy were −78.1 kJ·mol^{-1} and −133.9 J·K^{-1}·mol^{-1}, respectively, and the thermodynamic properties of the alloys were obviously improved. Zhang *et al.* [94] studied the microstructure and hydrogen absorption/desorption properties of the $La_{10-x}RE_xMg_{80}Ni_{10}$ (x = 0 or 3; *RE* = Sm or Ce) alloys. It was found that the addition of Ce or Sm resulted in grain refinement, which greatly improved the reaction kinetics and reduced the initial dehydrogenation temperature and hydrogenation reaction enthalpy change. In addition, the favorable effect of Ce on the comprehensive hydrogen storage performance of the alloys was found to be stronger than that of Sm. Zhong *et al.* [95] found a Mg_3MNi_2 intermetallic phase in the $Mg_2Ni_{0.7}M_{0.3}$ (*M* = Al, Mn and Ti) alloys which coexisted with the Mg and Mg_2Ni phases. The Mg_3MNi_2 phase was conducive to hydrogen absorption/desorption, and the closer the M atomic radius was to the Mg atomic radius, the more favorable the formation of the Mg_3MNi_2 phase was. The dehydrogenation activation energy of the $Mg_2Ni_{0.7}Ti_{0.3}$ alloy was as low as −73.15 kJ·mol^{-1}. Moreover, the Mg_3MNi_2 phase also showed a positive effect on the corrosion resistance of the alloys. Chen *et al.* [96] also found that the addition of Pr, Sm and Nd rare-earth elements could improve the hydrogen absorption/desorption kinetics properties of Mg-based alloys. The as-cast $Mg_{89}RE_{11}$ (RE = Pr, Sm and Nd) alloy was with a multiphase microstructure which transformed into MgH_2 nanocrystalline with the uniform distribution of the rare-earth hydride nanoparticles after hydrogenation. The rare-earth hydride nanoparticles acted as catalysts to improve the hydrogen absorption/desorption rates of the alloys. The $Mg_{89}Sm_{11}$ alloy exhibited the lowest activation energy and the fastest hydrogen absorption/desorption rates. The hydrogen storage capacity was up to 5 wt% and the dehydrogenation activation energy was 135.280 kJ·mol^{-1}. For the effects of transitional metals, Cao *et al.* [97] found that the $Mg_{77}Ni_{23-x}Al_x$ (x = 0 - 9) alloys exhibited better low-temperatures hydrogen storage performance with the addition of Al. Al induced the formation of a AlNi phase in the alloy which produced many phase/grain boundaries, providing channels for H-atom diffusion and sites for hydride nucleation, and thus significantly reducing the activation energy of the alloys and providing good hydrogen absorption kinetics at low temperatures. At 150˚C, the hydrogen storage capacity of the $Mg_{77}Ni_{17}Al_6$ alloy reached 2.91 wt% within 10 min, and the hydrogenation activation energy was as low as 73.68 kJ·mol^{-1}.

In addition, extensive works on the catalyst doping to improve the hydrogen absorption/desorption properties of Mg-based alloys have also been carried out. For the doping of metals, Yong *et al.* [98] studied the effects of Zr, Ti and V based

on a series of Mg-Ce-Y-Ni + 10 wt% *M* (*M* = Zr, Ti, V) alloys. They found that Zr and V elements were more effective on reducing the thermodynamic stability of the alloys. The apparent activation energy increased in the following order: Zr (87.7 kJ·mol^{-1}) < V (89.1 kJ·mol^{-1}) < Ti (99.3 kJ·mol^{-1}). Chen *et al.* [99] found that the doping of Mn nanoparticles into MgH_2 could improve the dehydrogenation performance. Compared with MgH_2, the initial hydrogen desorption temperature of the MgH_2 + 10 wt% nano-Mn was reduced to 175˚C, and the hydrogenation activation energy was reduced from (72.5 ± 2.7) kJ·mol^{-1} to (18.8 ± 0.2) kJ·mol^{-1}. The hydrogen absorption started at room temperature, and 2.0 wt% of hydrogen was absorbed within 30 min at a low temperature of 50˚C. Meanwhile, the capacity of the MgH_2 + 10 wt% nano-Mn composite did not decay too much after 20 hydrogen absorption/desorption cycles, showing excellent cycling performance.

In addition to metals, metallic compounds have also been found to have good catalytic effects on the hydrogen absorption/desorption properties of Mg-based alloys. For example, Zhang *et al.* [100] doped MgO into MgH_2 which could hinder the growth of Mg crystals, thus reducing the hydrogen desorption temperature and accelerating the absorption kinetics at room temperature. Tian *et al.* [101] ball-milled V-based catalysts (V_2O_5, Fe-V and V-Ni oxides) with MgH_2 to produce composite materials, among which the Fe-V oxide doped composite showed the best performance. The initial dehydrogenation temperature of the MgH_2 + 7 wt% Fe-V composite was 200˚C, 128˚C lower than that of the pristine MgH_2. Moreover, the hydrogen absorption/desorption performance was greatly enhanced with the hydrogen absorption capacity of 5.1 wt% and the capacity retention of 97.2 % after 10 cycles. Wang *et al.* [102] synthesized the $2LiBH_4$-MgH_2-K_2TiF_6 composite which exhibited low dehydrogenation initial temperature, completely eliminated dehydrogenation incubation period and fast kinetics as well as low activation energy of 100.3 kJ·mol^{-1}. The composite containing excess $LiBH_4$ could completely absorb 9.4 wt% of H_2 at 200˚C.

Researchers have also revealed synergistic effects in some bimetallic catalysis which exhibited better catalytic effect than monometallic catalysis. For example, Yong *et al.* [103] found that the (Ce, Sm)$H_{2.73}$ particles generated in-situ after hydrogen absorption of the $Mg_{90}Ce_5Sm_5$ alloy had a significant catalytic effect on the hydrogen absorption/desorption kinetics performance of the Mg-based alloys, which was superior to that of the single Sm_3H_7. The $Mg_{90}Ce_5Sm_5$ alloy displayed excellent kinetics properties, absorbing 4.6 wt% of hydrogen within 10 min at 593 K and desorbing 5.0 wt% of hydrogen within 80 min at the same temperature. Jiang *et al.* [104] investigated the hydrogen diffusion behaviors of the Cu-Ni co-doped MgH_2 (101) surface by the First-principles calculation. It was found that both single atom (Cu or Ni) doping and Cu-Ni co-doping could be stable on the MgH_2 (101) surface. The Ni-doped MgH_2 (101) surface exhibited strong hydrogen absorption ability with stable hydrogen absorption sites located on the Ni atoms. The surface of the Cu-Ni co-doped MgH_2 could be well matched with itself to obtain additional hydrogen storage regions. Shang *et al.* [105] found that the

$2NaBH_4 + MgH_2$ hydrides doped with $3TiCl_3$-$AlCl_3$ exhibited excellent dehydrogenation kinetics because $3TiCl_3$-$AlCl_3$ changed the control mechanism of the second dehydrogenation step from a two-dimensional interface-controlled process to a two-dimensional nucleation and growth-controlled process. Liu *et al.* [106] found that the doping of metal-metal oxide Ni-Al_2O_3 hybrid catalyst with high stability was more effect than that of NiO or Al_2O_3. The initial dehydrogenation temperature of the MgH_2 + Ni-Al_2O_3 composite (190˚C) was much lower than that of MgH_2-NiO or MgH_2-Al_2O_3 (240˚C) or that of milled MgH_2 (298˚C). The enhanced hydrogen desorption kinetics were due to the fact that Ni/Al_2O_3 could act as an electron acceptor that captured the electrons in the Mg-H bond to destabilize MgH_2. Moreover, Hou *et al.* [107] introduced a low-cost biomass carbon (BC)-based nickel catalyst (Ni/BC) into the MgH_2 system and found that the synergistic effect of the Ni/BC catalyst greatly promoted the hydrogen absorption and desorption kinetics of MgH_2. It was shown that the Ni/BC catalysts uniformly distributed around MgH_2 could form Mg_2Ni/Mg_2NiH_4 in-situ, which acted as a "hydrogen pump" to promote the hydrogen diffusion at the Mg/MgH_2 interfaces. Meanwhile, the carbon layer with amazing electrical conductivity greatly accelerated the electron transfer. The MgH_2 + 10 wt% Ni/BC composite started to desorb hydrogen at 187.8˚C, 162.2˚C lower than that of pure MgH_2. The hydrogen desorption capacity of 6.04 wt% was achieved within 3.5 minutes at 300˚C, and hydrogen absorption capacity of 5 wt%H_2 was achieved within 60 minutes under 3 MPa hydrogen pressure and 125˚C. Tome *et al.* [108] found that the co-catalysis of Ni-ZrO_2 significantly enhanced the hydrogenation and dehydrogenation properties of MgH_2. The apparent activation energy of dehydrogenation was 63.4 $kJ{\cdot}mol^{-1}$, which was 80.1 $kJ{\cdot}mol^{-1}$ lower compared to MgH_2. The MgH_2 + 5 wt% Ni + 5 wt% ZrO_2 nanocomposite exhibited better dehydrogenation and hydrogenation kinetics at 310˚C, with the hydrogen desorption capacity of 6.83 wt% and hydrogen absorption capacity of 6.10 wt% within 30 min. Yu *et al.* [109] found that the in-situ formed MgH_2Ni@CeO_2 composite by introducing Ni@CeO_2 into MgH_2 exhibited excellent absorption/desorption kinetics performance and good cycling stability. The unique Ni@CeO_2 coating structure contributed to the homogeneous distribution of the synergistic $CeH_{2.73}$ and Mg_2NiH_4 catalytic sites in the subsequent ball milling process. The composites absorbed 4.1 wt% of H_2 in 60 min at 100˚C and desorbed 5.44 wt% of H_2 within 10 min at 350˚C. Ren *et al.* [110] designed a core-shell Ni/Fe_3O_4@MIL additive to assist the hydrogen absorption (desorption) reaction of the MgH_2/Mg system through the co-catalysis of in-situ generated Mg_2NiH_4/Mg_2Ni and Fe. During the hydrogen absorption/desorption process, the synergetic effects of the reversible conversion of Mg_2NiH_4/Mg_2Ni and the stable catalyst of Fe weakened the Mg–H bond, thus reducing the dehydrogenation temperature and activation energy. The initial hydrogen desorption temperature of the MgH_2-Ni/Fe_3O_4@MIL composites was reduced from 613 K to 517 K with a hydrogen absorption capacity of 4.17 wt% under 3.0 MPa H_2 and 373 K. Meanwhile, the unique core-shell structure of the Ni/Fe_3O_4@MIL not only

provided reaction sites, but also prevented the agglomeration of nanoparticles and maintained a stable catalytic activity.

Compositing Mg-based alloys or hydrides with other types of hydrogen storage alloys has also been applied to modify the hydrogen storage alloys of Mg-based alloys. For example, Song *et al.* [111] alloyed the Mg_2Ni with RE-Mg-Ni to form Mg_2Ni-$REMg_2Ni$ (*RE* = La, Pr, Nd = 0 - 30) composites and found that the reversible hydrogen absorption and desorption capacity of the Mg_2Ni alloy with the addition of $LaMg_2Ni$ was significantly higher than that of pure Mg_2Ni alloy, and reached the maximum value when 20% $LaMg_2Ni$ was added; The hydrogen desorption rate of all the composites was higher than that of the pure Mg_2Ni alloy. Among them, the Mg_2Ni-20%$PrMg_2Ni$ composite displayed the highest hydrogen desorption plateau pressure at 250˚C and 200˚C and as well as the best diffusion performance. Meena *et al.* [112] found that alloying with 25 wt% $La_{23}Nd_{8.5}Ti_{1.1}Ni_{33.9}Co_{32.9}Al_{0.65}$ could decrease the activation energy of the MgH_2 nanocomposites by 98 $kJ{\cdot}mol^{-1}$ and increase the hydrogen storage capacity.

In addition to element/composite modification, treatments such as ball milling, annealing, rapid quenching etc. are widely used to prepare amorphous/nanocrystalline Mg-based alloys to improve the hydrogen absorption/desorption properties [113]. Zhang *et al.* [114] have found that ball milling could result in the nanocrystal structure in Mg-based alloys with high concentration of defects, which is essential for achieving good hydrogen absorption kinetics performance at room temperature. In addition, the impact of defect concentration on hydrogen absorption is stronger than microcrystal size. Wen *et al.* [115] applied the method of annealing coupled with cold forging processing to produce a cracked microstructure with the mixture of the Mg_2Ni fine grains (favorable for desorption) and Mg texturized grains (favorable for absorption) in Mg-based alloys, which significantly improved the hydrogen absorption/desorption kinetics. Chen *et al.* [116] investigated as-cast and extruded $Mg_{4.7}Y_{4.1}Nd_{0.5}Zr$ alloys, and found the extruded alloy exhibited superior hydrogen desorption kinetics and was able to desorb more than 6 wt% hydrogen within 15 min at 350˚C.

4. Ti-Based and Zr-Based Hydrogen Storage Alloys

Ti-based hydrogen storage alloys include AB_2-type Laves phase alloys and AB-type BCC phase alloys, and Zr-based hydrogen storage alloys are mainly AB_2-type Laves phase alloys. Most of AB_2-type alloys are of multiphase structure and the typical phases are Cl4-type and Cl5-type phases with the theoretical hydrogen storage capacity ranging from 1.8 wt% to 2.4 wt%. AB-type alloys usually have CsCl phase structure, and a representative is TiFe alloy. Its theoretical hydrogen storage capacity is 1.86 wt% and the equilibrium hydrogen pressure at room temperature is 0.3 MPa. Although both AB_2-type and AB-type alloys have relatively high theoretical hydrogen storage capacity, the former suffers from difficult activation and poor kinetics properties, and the latter have problems of difficult initial activation, high tendency to be poisoned and poor reversibility due to the low

equilibrium pressure at room temperature [24] [117] [118].

4.1. Zr-Based AB_2-Type Hydrogen Storage Alloys

Typical Zr-based AB_2-type hydrogen storage alloys include Zr-V, Zr-Cr, Zr-Ni and Zr-Mn alloys. Among these types of alloys, ZrCr2, ZrMn2, and ZrNi2 have MgZn2-type structure (hexagonal structure), and ZrV2 has MgCu2-type structure (Cubic structure) as shown in **Figure 4(a)**, **Figure 4(b)**. Zr-V-based AB_2-type alloys usually have fast hydrogen absorption/desorption rate, but are difficult to be prepared and have high hydrogen desorption residue; Zr-Cr-based alloys can form stable hydride and have long cycle life, but are difficult to be activated. Zr-Ni-based alloys have high hydrogen storage capacity (2.0 wt% H2) and a stable structure, but are poor in hydrogen absorption/desorption reversibility. Zr-Mn-based alloys can absorb hydrogen under the pressure below 1 bar and room temperature, but are with high cost [8] [119].

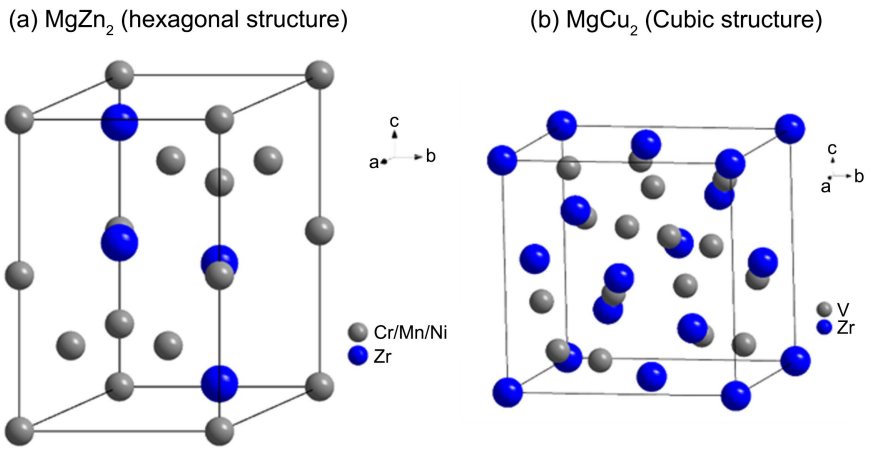

Figure 4. Crystal structures of Zr(Cr/Mn/Ni)2 (a) and ZrV2 (b).

Aiming at the above problems, many studies have been carried to improve the overall hydrogen storage properties of Zr-based AB_2-type alloys, among which elemental modification is one of the most common and effective methods. For example, for the modification of A-side elements, Matsuyama *et al.* [120] studied the effects of partial substitution of Ti for Zr in the $Zr_{1-x}Ti_xNi$ alloys ($0.05 \le x \le 0.5$). The alloys exhibited single discharge plateau for $0 \le x \le 0.2$ while double discharge plateaus for $x \ge 0.3$. The discharge plateau potentials shifted towards negative value with increasing Ti content. The *HRD* and cycling performance of the alloys were improved with higher Ti content. Wan *et al.* [121] studied the $Zr_{1-x}Ti_xLa_{0.03}Ni_{1.2}Mn_{0.7}V_{0.12}Fe_{0.12}$ ($x = 0.12$ - 0.22) alloys, and found that the $x = 0.12$ alloy exhibited excellent reversible discharge capacity of 466 $mAh \cdot g^{-1}$, and the $x = 0.22$ alloy had good cycling stability and large current discharge capability with a S_{500} of 71% and a HRD_{400} of 71%. They also studied the function of rare-earth elements on Zr-based $Ti_{0.2}Zr_{0.8}La_{0-0.05}Ni_{1.2}Mn_{0.7}V_{0.12}Fe_{0.12}$ alloys [122]. La could improve the activation performance of the alloys due to the catalytic effect of the

LaNi hydride, but it also caused a decrease in the discharge capacity and cycling stability. The $Ti_{0.2}Zr_{0.8}La_{0.03}Ni_{1.2}Mn_{0.7}V_{0.12}Fe_{0.12}$ alloy exhibited a C_{max} of 420 mA·g^{-1}, a $HRD_{0.71}$ of 79 % and a S_{500} of 63%. Leng *et al.* [123] tried to change the ratio of Zr content from $x = 3$ to $x = 9$ for the Zr_xV_5Fe ($x = 3$ - 9) alloys and found that with the increase of Zr content, the α-Zr phase abundance increased and the C15-ZrV_2 phase abundance decreased with the decrease of the hydrogen absorption plateau pressure. The C15-ZrV_2 phase in the Zr_7V_5Fe alloy displayed the lowest hydrogen absorption plateau pressure at room temperature, and the hydrogen absorption kinetics curves at 623 K indicated that the Zr_7V_5Fe alloy with the smallest average particle size and the largest phase boundary area exhibited the fastest hydrogen absorption reaction kinetics.

For the modification of B-side elements, Yao *et al.* [124] studied the partial substitution of V for Mn in the $ZrMn_{2-x}V_x$ ($x = 0$ - 0.8) alloys and found that the lattice parameters of the $ZrMn_2$ phase increased with increasing V content, resulting in a decrease in the dehydrogenation equilibrium pressure from 2.931 bar ($ZrMn_2$) to 0.080 bar ($ZrMn_{1.2}V_{0.6}$) at 200˚C, with a corresponding enthalpy change increasing from 43.29 kJ·mol^{-1} H_2 to 60.38 kJ·mol^{-1}. The $ZrMn_{1.2}V_{0.6}$ alloy exhibited excellent cycling stability with a stable hydrogen storge capacity of 1.63 wt% during 20 cycles. Wu *et al.* [125] studied the effects of partial substitution of V for Ni in the $ZrMgNi_{4-x}V_x$ ($x = 0$ - 2) alloys and found that the reversible hydrogen storage capacity gradually increased with increasing V content. Under 4 MPa H_2 pressure and 300 K, the $ZrMgNi_2V_2$ alloy absorbed 1.8 wt% H_2 in about 2 h without complicated activation process and reversibly desorbed the hydrogen in about 30 min at 473 K. Erika *et al.* [126] partially substituted Mo for Cr in the $ZrCr_{1-x}NiMo_x$ ($x = 0$ - 0.6) alloys and found that Mo could increase the Ni content in the secondary phase (Zr_7Ni_{10} relative to Zr_9Ni_{11}), which improved the *HRD* performance. Luo *et al.* [127] reported that partial substitution Mo for Co in the $ZrCo_{1-x}Mo_x$ ($x = 0$ - 0.2) alloys could significantly improve the initial activation behavior and the anti-disproportionation property, but the hydrogen storage capacity was decreased from 1.893 wt% ($x = 0$) to 1.66 wt% ($x = 0.2$), the plateau region of the *P-C-T* curves was shortened and the hydrogen desorption equilibrium pressure was decreased. Wu *et al.* [128] studied the effects of Ni addition in the $Zr(V_{1-x}Ni_x)_2$ ($x = 0.02$ - 0.25) alloys and reported that with the increase of Ni content, the hydrogen absorption capacity decreased and the equilibrium pressure increased. The $Zr(V_{0.05}Ni_{0.95})_2$ alloy exhibited good cycling stability at 823 K. Tu *et al.* [129] partially substituted Mn with Fe in the $ZrFe_{1.95-x}Mn_xV_{0.10}$ ($x = 0$ - 0.15) alloys and found that the increase of Mn content improved the activation properties of the alloys and reduced the hysteresis, but the plateau slope increased and the hydrogen storage capacity first increased and then decreased. At 243 K, the $ZrFe_{1.85}Mn_{0.10}V_{0.10}$ alloy displayed the highest hydrogen storage capacity of 1.69 wt% and the fastest hydrogen absorption rate with the $t_{0.9}$ of 46 s. Ai *et al.* [130] studied the $Zr_{56.97}V_{35.85}Fe_{7.18-x}Cr_x$ ($x = 0$, 3.59, 7.18) alloys and revealed that with the increase of Cr content, the diffusion activation energy was reduced due to the

increase of the cell volume of the C15-ZrV_2 phase. The hydrogen absorption capacity of the alloy was increased and the hydrogen absorption kinetics performance improved. The $t_{0.9}$ decreased from 90 s ($x = 0$) to 25 s ($x = 7.18$). Qin *et al.* [131] investigated the functions of Al addition in the $ZrFe_{2-x}Al_x$ ($x = 0.1, 0.2$) alloys and found that the alloys maintained high hydrogen storage capacity due to the presence of the Zr_2Fe impurity phase, which was inconsistent with a previous study that Al alloying caused a sharp decline in the hydrogen storage capacity.

Some studies also explored the phase function on the hydrogen storage properties of Zr-based AB_2-type alloys. Yao *et al.* [132] reported that the formation of metastable phases in the phase transition reaction of homogeneous structure could optimize the cyclic stability of this alloy system. It was found that the phase transformation of the $Zr_{0.8}Ti_{0.2}Co$ alloy during hydrogen absorption/desorption was from $Zr_{0.8}Ti_{0.2}Co_4Zr_{0.8}Ti_{0.21}CoH_3$ (heterogeneous structural phase transition) to $Zr_{0.8}Ti_{0.2}Co_4Zr_{0.8}Ti_{0.2}CoH_{1.4}$ (homogeneous structural phase transition). Therefore, the stable capacity was provided by the metastable phase $Zr_{0.8}Ti_{0.2}CoH_{1.4}$. By studying the co-substitution of Nb and Ni the in $Zr_{1-x}Nb_xCo_{1-y}Ni_y$ ($x, y = 0$ - 0.3) alloys, Yao *et al.* [133] proposed that the phase transition reaction of the thermodynamically homogeneous structure is an effective way to avoid disproportionation. Among them, the $Zr_{0.8}Nb_{0.2}Co_{0.8}Ni_{0.2}$ alloy exhibited an ultra-long cycle life with the S_{100} of 97.6%, as well as a high hydrogen storage capacity of 2.42 H (f.u.), which was the result of the synergistic effect of the homogeneous structure phase transition and the H-ordered migration mechanism (lamellar and linear de-embedding). Yu *et al.* [134] found that the main hydrogen-absorbing phases of the $Zr_{57}V_{36}Fe_7$ alloy were ZrV_2 and α-Zr phases; The hydride was with high stability, resulting in the difficulty for hydrogen desorption. But the alloy was with good pulverization resistance and air poisoning resistance. After being exposed in air for 2 h, both the hydrogen absorption rate and the hydrogen absorption capacity were decreased after 3 cycles. However, both the hydrogen absorption rate and the hydrogen absorption capacity could be largely recovered after reactivation for 1 h by pumping at 450˚C. It has also been pointed out that the electrochemical properties of AB_2-type alloys depend not only on the phase composition but also on the amount of a certain specific phase [122]. By studying the $ZrNi_{1.2}Mn_{0.5}Cr_{0.2}V_{0.1}$ alloy treated with different cooling rates, Solonin *et al.* [122] reported that the alloys with high content of Zr_7Ni_{10} phase could be activated faster, those with high C15 and C14 phase content displayed higher maximum discharge capacity, while those with lower Zr_7Ni_{10} phase content showed better cycling stability.

Treatments such as annealing, melt-spun, rapid solidification are also very effective to improve the hydrogen storage properties of Zr-based AB_2-type alloys [135]-[139]. For example, Wan *et al.* [139] reported that annealing treatment increased the maximum discharge capacity of the $Zr_{0.76}Ti_{0.24}Ni_{1.1}Mn_{0.7}V_{0.2}$ alloy from 350 $mAh \cdot g^{-1}$ to 400 $mAh \cdot g^{-1}$ and also improved the cycling stability and *HRD* performance. Lee *et al.* [136] also found that the $ZrV_{0.7}Mn_{0.5}Ni_{1.2}$ alloy annealed at 1000˚C for 12 h was with higher discharge capacity and better *HRD* performance

than the as-cast alloy. The improved high-rate discharge performance was due to the increase of Ni content in the matrix phase. Zhang *et al.* [137] compared the effects of annealing and melt-spun and found that the annealed $Zr_{0.9}Ti_{0.4}V_{1.7}$ alloy had a high hydrogen storage capacity of 2.83 wt% and fast hydrogen absorption kinetics after one cycle of activation, while the alloy after melt-spun performed better in the initial hydrogen absorption rate due to the increased alloy surface area and the grain refinement. But the amount of hydrogen storage was smaller. Luo *et al.* [138] compared the effects of different preparation processes on the hydrogen storage properties of the Zr-based Zr_7V_5Fe alloy. It was found that the annealed alloy had the lowest plateau pressure of about 0.02 Pa and the highest hydrogen storage capacity of about 1.4 wt% at 623 K; the melt-spun alloy and the melt-spun + annealed alloy could be activated without incubation, exhibiting excellent activation property; The melt-spun + annealed treated Zr_7V_5Fe alloy had the best hydrogen absorption kinetics property. Wijayanti *et al.* [139] studied the effect of rapid solidification process on the $Ti_{0.15}Zr_{0.85}La_{0.03}V_{0.12}Mn_{0.7}Fe_{0.12}Ni_{1.2}$ alloy. It was found that the grain size of the alloy decreased from the initial 3.5 mm to 250 nm with the increase of the cooling rate. The alloy with cooling rate of 16.5 Hz exhibited the highest discharge capacity of 414 $mAh{\cdot}g^{-1}$ due to its optimal two-phase structure containing C15 and C14 phases.

Surface coating is an effective method to improve the anti-poisoning ability of the Zr-based AB_2-type alloys. For example, Zhang *et al.* [140] found that homogeneous deposition of the Pd-Ag coating on the surface of the ZrV_2, $Zr_{0.9}Ti_{0.1}V_2$ and $Zr_{57}V_{36}Fe_7Zr$ alloys improved the anti-poisoning ability of the alloys in a wide temperature range. the Pd-Ag coating also resulted in the easy activation and accelerated the hydrogenation kinetics of the alloys.

4.2. Ti-Based AB_2-Type Hydrogen Storage Alloys

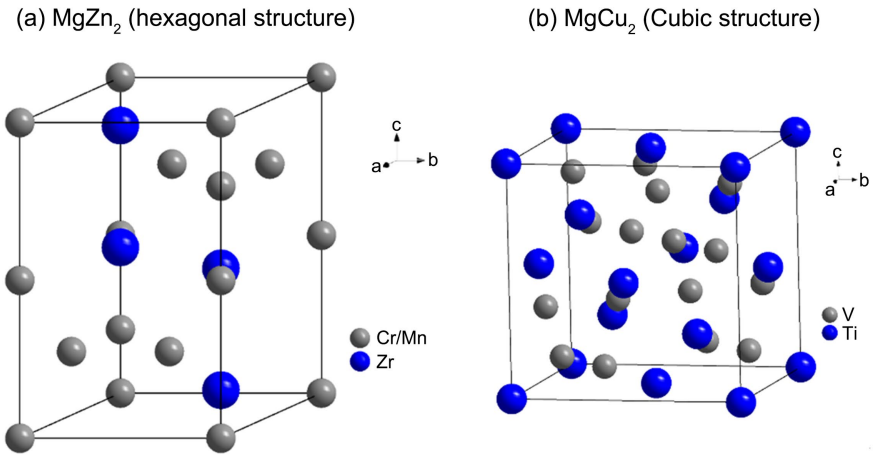

Figure 5. Crystal structures of Ti(Cr/Mn)2 (a) and TiV2 (b).

Ti-based AB_2-type hydrogen storage alloys mainly include Ti-Mn, Ti-Cr, and Ti-V alloys. Among these alloys, $TiMn_2$ and $TiCr_2$ have $MgZn_2$-type structure

(hexagonal structure), and TiV_2 has $MgCu_2$-type structure (Cubic structure) as shown in **Figure 5**. The hydrogen storage capacity of Ti-based AB_2-type alloys can reach 2.6 wt% under atmospheric pressure and room temperature. Among them, the Ti-Mn alloy can be readily activated under room temperature, but the alloy particles are easily pulverized and thus the cycle stability is poor. The Ti-Cr alloys can also absorb hydrogen readily but has some shortcomings such as high plateau pressure, low hydrogen absorption capacity, slow heat transfer rate and large hysteresis. The Ti-V alloys have high hydrogen storage capacity but poor activation and dehydrogenation properties [26]. Focusing on Ti-based AB_2-type hydrogen storage alloys, various modifications have been carried out including elemental subsitution, annealing, ball milling etc.

For elemental substitution, Han *et al.* [141] used Zr to partial substitute for Ti in the $Ti_{7-x}Zr_xV_5Fe$ (x = 0 - 2.1) alloys which contained α-Zr and C15-ZrV_2 phases. Withthe increase of Ti content, the C15-ZrV_2 phase abundance first increased and then decreased, while the opposite was true for the α-Zr phase; The plateau pressure of the α-Zr phase increased with the increase of Ti content, while that of the C15-ZrV_2 phase showed the opposite trend. Therefore, the stoichiometric ratio of A/B might play a key role in determining the plateau pressure of the two phases. Zhang *et al.* [142] found that Zr could refine the nano-eutectic texture of the $Ti_{40}Zr_{60-x}V_x$ (x = 20 - 30) alloys with ultra-fine nano-eutectic structures of 50 - 500 nm between lamellar layers. The alloys exhibited excellent activation and hydrogenation properties but low reversible hydrogen storage capacity. The $Ti_{40}V_{35}Zr_{25}$ alloy achieved the highest hydrogen absorption capacity of 2.4 wt% within 10 min under1 MPa H_2 and 200˚C. Cao *et al.* [142] studied the effects of Mn on the $Ti_{0.85}Zr_{0.17}Cr_{1.2-x}Mn_xFe_{0.7}V_{0.1}$ (x = 0 - 0.3) alloys, and it was found that the plateau pressure and hydrogen storage capacity of the alloys increased with increasing Mn content. Moreover, they also found that the effects of Cr addition in the $Ti_{0.85}Zr_{0.17}Cr_{1.0+y}Mn_{0.2}Fe_{0.7}V_{0.1-y}$ (y = 0 - 0.10) alloys had similar effects to those of Mn except that the hydrogen storage capacity decreased with decreased slightly. The hydrogen absorption plateau pressure of the $Ti_{0.85}Zr_{0.17}Cr_{1.1}Mn_{0.2}Fe_{0.7}$ alloy was 5.08 MPa under 293 K and the desorption pressure was 24.90 MPa under 363 K. Yan *et al.* [143] studied the effects of partial substitution of Mo for Cr in the $(Ti_{0.85}Zr_{0.15})_{1.1}Cr_{1-x}Mo_xMn$ (x = 0.05 - 0.2) alloys. It was found that with the increase of Mo content, both the hydrogen absorption and desorption capacities decreased, and the plateau slope increased. The maximum hydrogen absorption capacity and desorption capacity was obtained for the $(Ti_{0.85}Zr_{0.15})_{1.1}Cr_{0.95}Mo_{0.05}Mn$ alloy which were 1.76 wt% and 1.09 wt%, respectively. Nygard *et al.* [144] substituted Fe for both Ti and V for the $(Ti_{0.7}V_{0.3})_{1-z}Fe_z$ (z = 0 - 0.3) alloys and found that the increase of Fe content reduced the enthalpy and activation energy contributing to the fast kinetics property. Pineda *et al.* [145] reported that the addition of Al in the $Al_x(TiVNb)_{1-x}$ (x = 0.05 - 0.25) alloys decreased the lattice parameters thus reducing the hydrogen storage capacity. The x = 0.05 alloy showed relatively high hydrogen storage capacity (2.96 wt%) and its hydride was less stable.

Compared with the ternary TiVNb alloy, it had lower initial hydrogen desorption temperature of about 100˚C and the enhanced reversible hydrogen storage capacity of 1.76 H/M (2.83wt %). Zhou *et al.* [146] studied a series of low-cost and low-V $Ti_{0.95}Zr_{0.05}Mn_{0.9+x}Cr_{0.9+x}V_{0.2-2x}$ (x = 0 to 0.02), $Ti_{0.93}Zr_{0.07}Mn_{1.1+y}Cr_{0.7+z}V_{0.2-y-z}$ (y = 0, 0.05, z = 0.002, 0.05) and $Ti_{0.93+w}Zr_{0.07}Mn_{1.15}Cr_{0.7}V_{0.15}$ (w = 0.002, 0.04) alloys. It was found that the decrease of V content led to the increase of plateau pressure but decreased the plateau slope. The addition of super-stoichiometric Ti resulted in the expansion of cell volume and the improvement of hydrogen affinity, which reduced of hydrogen absorption/desorption plateau pressure and hysteresis. The $Ti_{0.95}Zr_{0.07}Mn_{1.15}Cr_{0.7}V_{0.15}$ alloy was with a hydrogen absorption capacity of 1.83 wt% under 3.2 MPa H_2 pressure and 10˚C and a hydrogen desorption capacity of 1.07 wt% at 90˚C. Bing *et al.* [147] developed a Ti-Zr-Cr-based $(Ti_{0.8}Zr_{0.2})_{1.1}Mn_{1.2}Cr_{0.55}Ni_{0.2}V_{0.05}$ alloy with the inclusion of Mn, Ni and V elements, which displayed good thermodynamic and kinetics properties. The alloy could desorb hydrogen under ambient conditions of 1 - 40 atm and 273 - 333 K. The hydrogen storage capacity of the alloy was 1.82 wt% at 298 K, and the hydrogen absorption and desorption plateau pressure were 10.88 and 4.31 atm, respectively. Wijayanti *et al.* [148] changed the ratio between A (Ti, Zr) and B (Mn, V, Fe, Ni) components and found that $AB_{1.9}$ alloy with substoichiometry had a high discharge capacity of 495 $mAh{\cdot}g^{-1}$. The increase of the B/A ratio significantly increased the hydrogen desorption equilibrium pressure from 0.3 bar (B/A = 1.9) to 0.8 bar (B/A = 2.0) at 293 K. The $AB_{1.95}$ alloy exhibited the best activation properties and *HRD*, and the $AB_{2.0}$ alloy exhibited excellent cycling stability and a high hydrogen diffusion coefficient. Khajavi *et al.* [149] studied the effects of both elemental substitution of Fe for Mn and annealing treatment of the $Ti_{0.5}Zr_{0.5}(Mn_{1-x}Fe_x)Cr$ (x = 0 - 0.4) alloys. XRD results showed that neither Fe addition nor annealing treatment changed the multiphase structure of the alloys, and the main phases had the same hexagonal structure. But the lattice parameters significantly decreased with increasing Fe content.

In addition to elemental modification, microstructures and hydrogen storage properties can also be tailored by applying different preparation methods and subsequent treatments. For example, Stepanova *et al.* [150] prepared the $Ti_{6.5}Al_{3.5}Mo_{1.5}Zr_{0.3}Si$ alloy with refined the texture using the electron beam melting method, and microhardness of alloy was also found to decrease with increasing beam current, but the hydrogenation process increased the alloy hardness due to the precipitation of the δ-TiH hydride and the redistribution of the alloy elements (formation of intermetallic particles). After the treatment with the beam current of 3 mA and the scanning speed of 150 $mm{\cdot}s^{-1}$, the sample exhibited the highest hydrogen absorption rate of 0.006 $wt\%{\cdot}min^{-1}$. Khajavi *et al.* [151] found that ball milling and cold rolling could recover the alloys after exposion to air. The $Ti_{0.5}Zr_{0.5}(Mn_{1-x}Fe_x)Cr$ (x = 0 - 0.4) alloys could not absorb hydrogen after 10 days of air exposure, but could quickly recover the hydrogen absorption and desorption ability after mechanical deformation such as a short period of ball milling or

a single pass of cold rolling. Moreover, ball milling could result in fast kinetics but also lead to the loss of hydrogen storage capacity. Comparatively, cold rolling provided faster kinetics and minimal capacity loss and was considered to be an appropriate treatment for the recovery of the alloys after exposion to air. Liu *et al.* [152] prepared the Cd/Pd particles with special core/shell microstructure by a two-step reduction method which was further ball milled with the $Ti_{49}Zr_{26}Ni_{25}$ alloy. The Cd/Pd composite coated on the $Ti_{49}Zr_{26}Ni_{25}$ alloy surface could reduce the charge transfer resistance and accelerate the hydrogen transfer of the $Ti_{49}Zr_{26}Ni_{25}$ alloy, thus improving the electrochemical performance and reaction kinetics of the alloy electrode. The $Ti_{49}Zr_{26}Ni_{25}$ + 7 wt% Cd/Pd electrode showed the highest discharge capacity of 272.9 $mAh{\cdot}g^{-1}$ and the $Ti_{49}Zr_{26}Ni_{25}$ + 5 wt% Cd/Pd electrode showed the best cycling stability.

4.3. Ti-Based AB-Type Hydrogen Storage Alloys

A typical representative of AB-type hydrogen storage alloys is TiFe alloy, an intermetallic compound being widely studied at present. The structure of TiFe alloy belongs to body centered cubic (BCC) structure as shown in **Figure 6**. TiFe and TiFe-based alloys generally have the advantages of high hydrogen storage capacity (1.86 wt%), excellent cycling stability, rapid hydrogen absorption/desorption kinetics in a wide temperature range, and high abundant with low cost [153]-[155]. However, the activation difficulty and large hysteresis during hydrogen absorption/desorption have been limiting the application of this alloy system. To solve the above problems, intensive efforts have been made to understand the hydrogen storage properties and the development methods of this alloy system [9] [154].

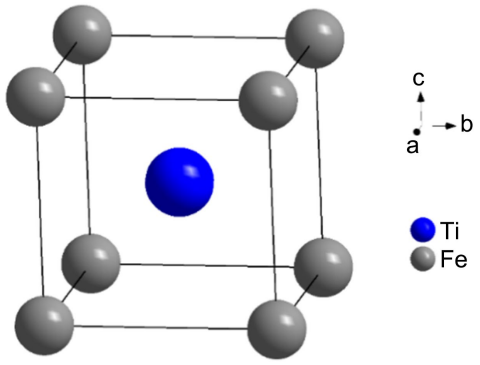

Figure 6. Crystal structure of TiFe alloy.

Elemental substitution and addition can moderate the hydrogenation behavior of TiFe-based hydrogen storage alloys by optimizing their microstructure and phase composition. The substitution and addition of rare-earth elements in TiFe-based alloys usually increase the alloy phase boundary, refine the crystal size, shorten the activation incubation period, and significantly improve their activation properties. Zhai *et al.* [156] found that adding an appropriate amount of La could improve the hydrogen absorption kinetics of the $Ti_{1-x}La_xFe_{0.8}Mn_{0.2}$ (x = 0 -

0.09) alloys. The hydrogen storage capacity reached the maximum of 1.633 wt% at 323K when $x = 0.01$, and the plateau pressure increased with the substitution of La for Ti. Liu *et al.* [157] reported that the $Ti_{1.1-x}Fe_{0.6}Ni_{0.3}Zr_{0.1}Mn_{0.2}La_x$ ($x = 0$ - 0.08) alloys with La addition showed excellent activation performance, and can be fully activated within one cycle Han *et al.* [158] found that the addition of Y significantly improved the activation properties and hydrogen absorption/desorption kinetics of the $Ti_{1.1-x}Zr_{0.1}Y_xFe_{0.6}Ni_{0.3}Mn_{0.2}$ ($x = 0$ - 0.08) alloys which could be fully activated by hydrogen absorption under 3 MPa H_2 pressure and 150˚CC, and also exhibited a fast hydrogen absorption rate at 10 C. When $x = 0.02$, the saturated hydrogen absorption rate of the alloy reached 92%, and the maximum hydrogen absorption capacity at 70 °C was 1.704 wt%. Zhang *et al.* [159]. Partially substituted Sm for Ti in the $Ti_{1.1-x}Fe_{0.6}Ni_{0.1}Zr_{0.1}Mn_{0.2}Sm_x$ ($x = 0$ - 0.08) alloys which refined the grain size and thus improved the activation performance and greatly shortened the activation incubation period. All the alloys exhibited good activation property and could be fully activated under room temperature. Particularly, the $x = 0.04$ and $x = 0.08$ alloys absorbed hydrogen without incubation time, and the hydrogen storage capacity of the $x = 0.02$ alloy at 313 K reached 1.438 wt%. Xu *et al.* [160] reported that the substitution of Pr for Ti in the $Ti_{1.1-x}Pr_xFe_{0.6}Ni_{0.3}Mn_{0.2}$ ($x = 0$ - 0.08) alloys greatly improved the cycling performance. When $x = 0.08$, the S_{50} of the alloy electrode reached 90.42%. Shang *et al.* [161] found that the $Ti_{1.1-x}Fe_{0.7}Ni_{0.1}Zr_{0.1}Mn_{0.1}Pr_x$ ($x = 0$ - 0.08) alloys with Pr partially substituting for Ti at $x = 0.04$ and 0.08 displayed good activity property, and could absorb hydrogen without any incubation time. Meanwhile, Pr addition was also beneficial to the nucleation rate and grain refinement, thus enhancing the hydrogenation kinetics of the alloys. At 313 K, the hydrogenation capacity of the $x = 0.02$ alloy reached a 1.438 wt%.

The addition of transitional elements usually induces the formation of secondary phases with catalytic effect on the activation performance of TiFe-based alloys. Lee *et al.* [162] found a small amount of $TiFe_2$ phase with C14 Laves structure and Ti_2Fe phase with cubic structure appearing in the Zr- and ZrCr-containing TiFeZr and TiFeZrCr alloys. Because $TiFe_2$ and Ti_2Fe phases have higher microstrain, more dislocations and smaller grain size than the TiFe main phase, the TiFeZr and TiFeZrCr alloys exhibited easy activation performance under 30 bar H_2 pressure and room temperature. Li *et al.* [163] reported that partial substitution of Fe for Ni could significantly reduce the minimum activation temperature. Among the $TiFe_{1-x}Ni_x$ ($x = 0$ - 0.4) alloys, the lowest activation temperature was obtained for the $x = 0.4$ alloy which was 443 K. Further studies showed that the decrease of activation temperature was attributed to the presence of NiO in the nickel-containing alloys which reduced the compactness of the surface oxide film. Moreover, it was found that the plateau pressure decreased and the hydride stability increased with increasing Ni content. Dematteis *et al.* [164] studied the effects of microstructure change and secondary phase formation on the activation and kinetics performance of the TiFe alloy by partial substitution of Mn and Ti for Fe.

It was found that the secondary phase reacted with hydrogen which enhanced the activation performance and allowed hydrogen absorption under mild conditions. However, the large number of secondary phases reduced the hydrogen storage capacity and reversible capacity of the alloys. A good compromised was reached for the $TiFe_{0.85}Mn_{0.05}$ alloy which displayed the best comprehensive hydrogen absorption/desorption performance with a reversible capacity of 1.63 wt% (under 0.03 - 2.5 MPa H_2 pressure and 25˚C), easy activation (incubating at 25˚C and 2.5 MPa H_2 pressure for 6 hours) and good kinetics performance. The alloy exhibited a fast hydrogen absorption rate with the t_{90} less than 2 min. Dematteis *et al.* [165] studied the effects of substitution of Cu for Fe in the $TiFe_{0.88-x}Mn_{0.02}Cu_x$ (x = 0 - 0.04) alloys. It was found the alloys were of multiphase structure with the secondary phases of β-Ti and Ti_4Fe_2O phases. The secondary phase abundance increased with the addition of Cu content. A small amount of secondary phase was helpful for the hydrogen absorption activation while the reversible capacity was reduced and the activation conditions became more stringent with the further increase of the secondary phase amount. Further study showed that the decrease in the capacity was attributed to the increase in the pressure difference between the first and second plateaus of the intermetallic compounds caused by Cu substitution which decreased the first plateau pressure while increases the second plateau pressure. Ali *et al.* [166] studied the effects of substituting Cu for Y of the $TiFe_{0.86}Mn_{0.1}Y_{0.1-x}Cu_x$ (x = 0.01 - 0.09) alloys. Results showed that with the increase of Y content, the hydrogen storage capacity first increased and then decreased with the maximum value of 1.89 wt% at x = 0.05. Moreover, the plateau pressure and the plateau slope decreased with Cu addition. Li *et al.* [167] found that the addition of Zr in $Ti_{1.08}Y_{0.02}Fe_{0.8}Mn_{0.2}Zr_x$ (x = 0 - 0.08) alloys significantly shortened the activation period, and the x = 0.04 alloy could be directly activated without inoculation time. But excessive Zr led to the formation of precipitates, which reduced the hydrogen absorption/desorption capacity of the alloys. Faisal *et al.* [168] studied the binary TiFe alloy and eight ternary Ti-Fe-V alloys with 3 wt% Ce addition. It was found that the addition of Ce promoted the activation property of the alloys at room temperature by inhibiting the formation of the $Ti_4Fe_2O_{1-x}$ oxides and adjusting the phase composition. V addition could improve the available hydrogen storage capacity of the alloys. Among the designed Ti-Fe-V series alloys, the $Ti_{46}Fe_{47.5}V_{6.5}$ alloy displayed the best hydrogen storage performance with the available hydrogen capacity of about 1.5 wt% under 1 MPa hydrogen absorption pressure and 0.1 MPa hydrogen desorption pressure at 30˚C. Leng *et al.* [169] tried to adjust the amount of Co in the $TiFe_{0.8}Mn_{0.2}Co_x$ (x = 0 - 0.15) alloys which improved the alloys' hydrogen storage capacity. With the increase of Co content, the lattice parameters and hydrogen storage capacity of the TiFe phase decreased, but the improvement of the flatness on the hydrogen desorption plateau increased the available hydrogen capacity of the alloys. Further research showed that the increase in the available hydrogen capacity might be owning to the adjustment of the change of the octahedral interstitial environment caused by Mn appearance in

the TiFe phase, which helped improve the flatness of α-β desorption plateau. Shang *et al.* [170] found that the addition of super-stoichiometric Ti in TiFe alloy led to the decrease of hydrogen storage capacity, kinetics performance and dehydrogenation utilization rate of the alloys. Further substitution of Mn for Fe reduced the average grain size, which benefited the activation, improved the hydrogen storage capacity and kinetics performance, and led to a slight increase in the dehydrogenation enthalpy value. The $Ti_{1.14}Fe_{0.8}Mn_{0.2}$ alloy exhibited the highest hydrogen absorption capacity of 1.764 wt%, the shortest saturated hydrogen absorption time of 300 s, and a high dehydrogenation utilization rate of 96.9%.

As activation is one of the main obstacles faced with TiFe-based alloys, extensive works have been done focusing on ameliorating the activation property of this alloy system. For example, Liu *et al.* [171] reported that the addition of an appropriate amount of high oxygen could improve the initial hydrogen absorption of TiFe alloy. The TiFe-$O_{3.78}$ composite was fully activated after two hydrogen absorption/desorption cycles at room temperature. Further studies showed that high oxygen content would lead to the formation of the Ti_4Fe_2O phase in TiFe alloy, thereby improving the activation kinetics. However, the reduction of the TiFe phase content decreased the hydrogen storage capacity. Doping catalysis is another important means to improve the activation performance of TiFe-based alloys. Alam *et al.* [172] reported that doping a small amount of metal La into TiFe alloy could effectively reduce the activation incubation period. Under 40 bar hydrogen pressure and room temperature, the first hydrogen absorption capacity reached 1 wt% in less than 5 min. Lv *et al.* [173] added different amounts of $ZrMn_2$ to the TiFe alloy to produce TiFe + x wt% $ZrMn_2$ (x = 2 - 12) composites. The composites were composed of TiFe main phase and Zr-rich and Mn-rich secondary phases. The secondary phase abundance increased with the increase of $ZrMn_2$ addition. Due to the very fine distribution of the secondary phase, the first hydrogenation kinetics and hydrogen storage capacity increased, and the plateau pressure decreased. Moreover, the synergistic effect of Zr, Mn, V and other elements improved the kinetics properties and hydrogen storage capacity. Patel *et al.* [174] added Zr, Mn and Zr + Mn to TiFe alloy and it was found that the addition of enabled the activation under 20 bar hydrogen pressure and room temperature, but the kinetics was very slow. The alloy with 2 wt% Zr was not activated. When 4 wt% Zr was added, the alloy absorbed 1.2 wt% hydrogen. However, when Zr and Mn were added together, the alloy with 1 wt% Mn + 2 wt% Zr exhibited better kinetics than the alloy with only Mn or only Zr. The maximum hydrogen storage capacity reached within 7 h, which was also higher (about 1.8 wt%). The composite doped with 4 wt% Zr + 2 wt% Mn exhibited a hydrogen absorption capacity of 2 wt% within 5 hours. Moreover, Patel *et al.* [175] further added V, Zr + V and Zr + V + Mn into TiFe alloy. it was found that the alloys with (Zr, V) and (Zr, V, Mn) demonstrated rapid activation performance which might be enabled by the existence of the Ti_2Fe-like secondary phase acting as the entrance for hydrogen atoms. However, the TiFe alloy with 2 wt% V could not be activated at room

temperature, and the that with 2 wt% Zr alone was ineffective, neither, which meant that there were some synergistic effects when Zr and V were added simultaneously.

Appropriate ball milling process can refine the grain size and even induce an amorphous structure, which generates cracks on the alloy surface and increases the hydrogen diffusion channel. Shang *et al.* [176] synthesized a $Ti_{1.04}Fe_{0.7}Ni_{0.1}Zr_{0.1}Mn_{0.1}Pr_{0.06}$ + 10 wt% Ni composite with amorphous structure by ball milling. Owing to the decrease of particle size, grain refinement, increase of crystal defects and change of surface state, the alloy reached the maximum discharge capacity in the first cycle. However, with the increase of ball milling time, the discharge capacity and electrochemical kinetics properties of the composites decreased significantly. Li *et al.* [177] also found that ball milling treatment led to grain refinement, particle size reduction and disordered structure of the $Ti_{1.04}Fe_{0.7}Ni_{0.1}Zr_{0.1}Mn_{0.1}Pr_{0.06}$ alloy. The sample milled for 0.5 h showed the best hydrogen absorption and desorption kinetics and hydrogen storage capacity. Under 3 MPa H_2 pressure and 313 K, the hydrogenation capacity reached 1.626 wt% within 2158 s, and the activation did not require incubation time when the temperature increased to 423 K. Similarly, Yuan *et al.* [178] reported that the activation time of the ball-milled alloy was greatly shortened, and the nano-grain boundaries and the phase boundaries resulted from the secondary phase provided a large number of channels for hydrogen diffusion. At 443 K, the activation time of the ball-milled alloy (0.75 h) was only 4 min. However, due to the increase in the number and density of crystal boundaries, the hydrogen storage capacity decreased significantly from 1.387 wt% to 0.46 wt% at 323 K.

Heat treatment has also been attempted on TiFe-based alloys, but the effects were not so desired due to the decrease of secondary phase content. For example, He *et al.* [179] compared the as-cast and annealed TiFe-6 wt% $ZrCr_2$ alloys and found that both alloys were with the TiFe main phase, a small amount of $TiFe_2$ and Ti_2Fe secondary phases. But the $TiFe_2$ secondary phase was significantly reduced after annealing. Both the alloys could be hydrogenated under 31 bar hydrogen pressure and room temperature without harsh activation process, but the hydrogenation of the annealed sample required about 40 hours of incubation time. Further studies showed that the secondary phase ($TiFe_2$) which was reduced by annealing played a key role in the hydrogenation process at room temperature.

5. V-Based Solid Solution Hydrogen Storage Alloys

V-based solid solution alloys have BCC phase structure as shown in **Figure 7**. The positions for hydrogen storage include the tetrahedral interstitial position and the octahedral interstitial position. Most hydrogen atoms enter the tetrahedral interstitial position. Since there are 12 tetrahedral interstitials in each crystal cell, there are many interstitial positions suitable for hydrogen accommodation, so that the theoretical hydrogen storage capacity of V-based solid solution alloys is as high as 3.8 wt% [180]. The main representative of V-based alloys is V-Ti alloy, which has

the advantages of large hydrogen storage capacity and good kinetics performance. V-Ti alloy can absorb hydrogen at low plateau pressure or room temperature, but it has the disadvantages of difficult activation and poor reversibility with the desorption capacity of only half of the hydrogen absorption capacity at room temperature [91] [181]. Moreover, it is also costly.

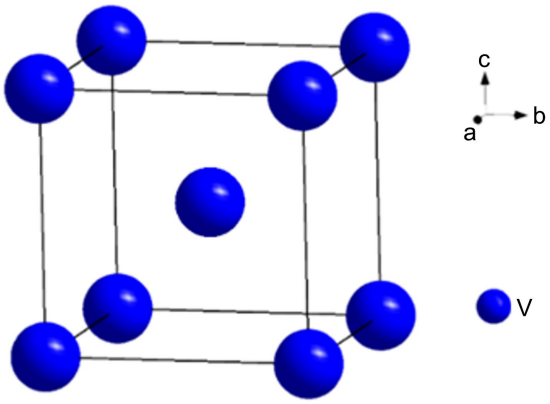

Figure 7. Crystal structure of V.

The addition of rare-earth elements and transitional metal elements can moderate the phase abundance and constituents, promote the synergistic effect between phases, and improve the hydrogen storage properties of the V-based alloys. For example, Chen *et al.* [182] found that the substitution of Ce for Mn in the $Ti_{33}V_{37}Mn_{30-x}Ce_x$ (x = 0 - 0.6) alloys led to the formation of Ce/CeO_2, increased the BCC phase abundance and decreased the C14 Laves phase abundance which improved the activation property and hydrogen absorption capacity. The alloy with Ce could absorb hydrogen without activation at high temperatures, which meant that the effect of Ce/CeO_2 on the activation of the alloys was stronger than that of the C14 Laves phase. The maximum hydrogen absorption capacity and hydride stability of the alloys increased with the increase of Ce content. The hydrogen absorption capacity and effective hydrogen storage capacity of the $Ti_{33}V_{37}Mn_{29.4}Ce_{0.6}$ alloy reached the maximum value of 3.35 wt% at 293 K and 2.25 wt% at 423 K, respectively. Xue *et al.* [183] also found a small amount CeO_2 phase among the BCC main phase in the $TiCr_3V_{16}Ce_x$ (x = 0 - 1) alloys. The addition of Ce increased the plateau pressure, while decreased the hydrogen storage capacity. The alloys with $x \geq 0.2$ could absorb and desorb hydrogen at room temperature without activation. When x = 0.2, the alloy exhibited the best performance with the hydrogen absorption capacity as high as 3.69 wt%, and the effective dehydrogenation capacity of 2.29 wt% at 25˚C. Tong *et al.* [184] added Ce to the $V_2Ti_{0.5}Cr_{0.5}NiCe_x$ (x = 0 - 0.10) alloys, and also found that the activation performance as well as the cycle stability of the alloy electrodes was significantly improved, but the *HRD* performance was decreased. When x = 0.08, the highest discharge capacity of 409 $mAh \cdot g^{-1}$ was obtained. Kong *et al.* [185] compared the effects of Y, La, Ce and Nd on the $Ti_{14.7}Zr_{1.8}V_{43.8}Cr_{12.3}Mn_{6.9}Fe_{3.0}Co_{1.4}Ni_{14.7}Al_{1.2}RE_{0.2}$

alloy. It was found that Y increased the reversibility of hydrogen absorption and desorption. Ce promoted the BCC phase formation and discharge capacity, and reduced the surface charge transfer resistance at room temperature. Nd increased the C14 phase abundance, reduced the plateau pressure, and increased the hydrogen storage capacity, the discharge capacity and the hydrogen diffusion rate. But La reduced the discharge capacity, and hindered the activation and surface electrochemical reaction. Luo *et al.* [186] prepared the $V_{47}Fe_{11}Ti_{30}Cr_{10}RE_2$ (*RE* = La, Ce, Y, Sc) as-cast alloys with natural cooling. These alloys could be completely activated after only one hydrogen absorption/desorption cycle after pretreatment and the time required to absorb hydrogen to 90% saturation at room temperature was less than 100 s, demonstrating excellent hydrogen absorption kinetics. Further analysis indicated that the alloys were composed of nanocrystals with a large number of interfaces and grain boundaries. These defects could be used as effective channels for hydrogen atom diffusion. The $V_{47}Fe_{11}Ti_{30}Cr_{10}Y_2$ alloy exhibited a maximum hydrogen storage capacity of 3.41 wt% at 295 K.

For the function of transitional metals on the V-based solid solution alloys, Luo *et al.* [187] studied the effects of partial substitution of Al for Ti of the $V_{48}Fe_{12}Ti_{15-x}Cr_{25}Al_x$ (x = 0, 1) alloys which were with the BCC main phase, and the Ti-rich and TiFe minor phases. It was found that Al addition increased the lattice parameters of the BCC phase as well as the equilibrium pressure of hydrogen desorption, but reduced the hydrogen storage capacity. Moreover, reaction enthalpy for hydrogen desorption was decrease but the activation energy for hydrogen desorption was increased. Moreover, the addition of Al improved the kinetics of the hydrogen absorption/desorption. Chanchetti *et al.* [188] compared the effects of Fe, Co and Ni in the $Ti_{31}V_{26}Nb_{26}Zr_{12}M_5$ (M = Fe, Co, Ni) as-cast alloys. The alloys mainly composed of BCC phase and a small amount of C14 phase. After hydrogenation, all the alloys absorbed about 1.9 wt% hydrogen at room temperature. The XRD pattens of the fully hydrogenated sample showed a multiphase structure composed of FCC and C14 hydrides. Thermal desorption spectroscopy (TDS) showed a multi-step hydrogen desorption process with a wide temperature range and a low initial temperature. Moreover, the addition of these transitional elements with low affinity for hydrogen improved hydrogen desorption behavior of the alloys and significantly reduced the initial hydrogen desorption temperature.

Modifying the ratio of the elements with high hydrogen affinity to improve the hydrogen storage properties of V-based alloys has also been extensively studied. Hang *et al.* [189] improved the activation behavior and hydrogenation kinetics performance of the $Ti_{10+x}V_{80-x}Fe_6Zr_4$ (x = 0 - 15) alloys by partially substituting high-cost V with relatively low-cost Ti. The x = 5 alloy exhibited the shortest incubation time of only 12 s under 4 MPa initial H_2 pressure and 298 K. The x = 10 alloy showed the highest C_{max} of 3.61 wt%. In addition, with the increase of x, the equilibrium plateau pressure decreased due to the lattice expansion of the main phase. The hydrogen desorption capacity of the alloy with an ending pressure of 0.001 MPa first increased and then decreased with the maximum value of 1.94

wt% at $x = 5$, while that with an ending pressure of 0.1 monotonously decreased with the maximum of 1.6 wt% at $x = 0$. Balcerzak *et al.* [190] found that the addition of Cr could increase chemical activity and enhance the hydrogen storage performance of $Ti_{0.5}V_{1.5-x}Cr_x$ ($x = 0$ - 0.3) alloys by producing a small amount of Cr-based solid solution BCC phase which not only relieved the oxidation of the alloy but also provided new channels for hydrogen diffusion. In addition, Cr addition could also improve the cycle stability of the alloy electrodes. The S_{50} increased from 41% ($x = 0$) to 94% ($x = 0.3$). Hang *et al.* [191] found that in the $V_{40}Ti_{20-x}Zr_xCr_{24}Mn_8Fe_8$ ($x = 0$ - 4) alloys, partial substitution of Zr for Ti could improve the activation performance and hydrogen absorption capacity of the alloys. Under the condition of 4 MPa initial hydrogen pressure and 293 K, all the Zr-containing alloys absorbed hydrogen quickly without activation, and the hydrogen absorption capacity gradually increased with the increase of Zr content. When $x = 4$, the maximum hydrogen absorption of 2.38 wt% was obtained. The dehydrogenation kinetics of the alloys was also excellent, and the dehydrogenation could be completed within 10 min, but the effective dehydrogenation capacity and efficiency need to be improved. Mao *et al.* [192] studied the preparation of the $(FeV_{80})_{48}Ti_{26+x}Cr_{26}$ ($x = 0$ - 4) alloys with Ti compensation. When x reached 4 at%, the hydrogen absorption capacity of the alloy reached 3.3 wt%, and the desorption capacity was 2.0 wt% under 10^{-4} MPa H_2 pressure and room temperature.

Various preparation and treatment methods have also been applied to improve the hydrogen storage properties of V-based alloys. Chen *et al.* [193] studied the influence of annealing time (973 K, 2 h\8 h\72 h\water quenching) of the $Ti_{19}Hf_4V_{40}Mn_{35}Cr_2$ alloy. It was found that the lattice parameters of the BCC phase decreased with the increase of annealing time. The eutectic structure (BCC phase + C14 Laves phase) formed in the annealed alloys, and the coarse dendrite BCC phase transformed into equiaxed dendrite phase. The grain size also decreased which benefited to the diffusion of H atoms. The hydrogen absorption capacity of the annealed alloys at room temperature was significantly higher than that of the as-cast alloy. Due to the decrease of hydride stability after heat treatment, the dehydrogenation activation energy of the annealed alloy decreased to 66.26 KJ·mol^{-1}. Liu *et al.* [194] tried very short annealing time (1673 K, 1 min\5 min\30 min\water quenching) on the $Ti_{19}Hf_4V_{40}Mn_{35}Cr_2$ alloy. It was found that the proportion of BCC phase was increased and lattice parameters were decreased after annealing. The alloy annealed for 1 min was with the highest effective hydrogen storage capacity of 2.23 wt% and the fastest hydrogen absorption rate. Since annealing treatment reduced the stability of the metal hydride, the dehydrogenation enthalpy of the alloys decreased significantly.

Hydride powder sintering (HPS) method has successfully solved the problem of crucible material selection of traditional induction melting for the preparation of V-based alloys, which provides a direction for large-scale production. However, the formation of Ti-rich oxide phase by HPS method leads to the loss of Ti in the main BCC phase, which further decreases lattice volume and reduces the

hydrogen storage capacity. Therefore, the control of Ti oxide phase is the key of the HPS process. Chen *et al.* [195] found that the formation of Ti oxide phase could be reduced by adding LaH_3 to the $V_{40}Ti_{26}Cr_{26}Fe_8$ alloy during hydride powder combustion method. When the amount of LaH_3 was 3%, the content of Ti oxide phase disappeared, and the ability of the hydrogen absorption/desorption was enhanced. The hydrogen absorption and desorption capacities of the composite sintered at 1673 K for 6 h with the LaH_3 doping of 3 wt% reached 3.13 wt% and 1.97 wt%, respectively.

With the development of research, the process and mechanism of hydrogen storage of V-based alloys is gradually revealed. Silva *et al.* [196] studied the hydrogen absorption and desorption reaction process of the $(TiVNb)_{85}Cr_{15}$ alloy. It was found that lattice parameters of the BCC phase were changing with the change of hydrogen content. The coexistence of the two phases with the same structure and different hydrogen concentrations suggested the existence of miscibility gap, which would lead to the formation of intermediate BCC hydrides. The hydrogenation process is: alloy ↔ BCC solid solution ↔ BCC intermediate hydride ↔ FCC dihydride. Han *et al.* [197] studied the phase evolution process of the $V_{72}Ti_{18}Cr_{10}$ nanoalloy particles during hydrogen absorption/desorption. Results showed that the phase evolution process during hydrogenation was BCC → BCC hydride → FCC, and the formation of metastable BCT phase was inhibited, indicating that the limited particle size of the alloy in the range of 0.1 - 5 μm and fewer defects than ordinary alloy ingots would hinder the formation of BCT phase. After the first dehydrogenation, the metastable BCT phase appeared in the alloy. Therefore, it was considered that the defects generated during the hydrogenation process and subsequent dehydrogenation process might lead to the generation of the BCT phase.

6. High-Entropy Hydrogen Storage Alloys

In 2004, Yeh first proposed the concept of high-entropy alloy (HEA), which was found to have excellent mechanical properties, high thermal stability, strong corrosion resistance as well as some functional properties such as hydrogen absorption/desorption ability [198]. Thus, this alloy system has attracted much attention. High-entropy alloys are generally composed of five or more main elements with similar atomic percentages. The concentration of the constituent elements ranges between 5 at.% - 35 at.%, and the mixing entropy is greater than 1.61 R (gas constant, 8.314 J/(mol·K)) [199]. Due to the high mixing entropy, HEAs tend to form structures dominated by simple solid solutions, such as C14-type (FCC) Laves phase structure, solid solution (BCC) structure, and close-packed hexagonal (HCP) structure [200]. Therefore, HEAs are basically divided into two types: Laves phase hydrogen storage alloys and BCC solid solution hydrogen storage alloys [201]. HEAs with Laves phase structure usually have the advantages of easy activation and fast kinetics, while those with BCC solid solution structure usually have a relatively high hydrogen storage capacity. But most HEAs have high

thermal stability and poor reversibility, so it is necessary to develop new HEAs that are able to desorb hydrogen under room temperature or to reduce the hydrogen desorption temperature of the existing HEAs [202]-[204]. The design of HEAs are based on the criteria including valence electron concentration (VEC), dimensionless parameter, mixing enthalpy, atomic size difference etc. [202].

As the maximum H/M of transitional metal hydrides are 2, it was believed that higher ratios could only be obtained from rare earth-based alloys until Sahlberg *et al.* [205] achieved a H/M of 2.5 under 53 bar H_2 and 299˚C for a high-entropy TiVZrNbHf alloy which is equivalent to 2.7 wt% H_2. The high H/M is due to the lattice strain in the alloy, which benefits to accommodate hydrogen in the tetrahedral and octahedral interstitial positions. Since then, many studied have followed up. Chen *et al.* [206] developed a six-membered TiZrFeMnCrV HEA with a single C14 Laves phase structure, which exhibited ultrafast hydrogen absorption kinetics and could absorb 1.80 wt% hydrogen under 30˚C. This HEA also displayed excellent hydrogen absorption/desorption cycling performance with a stable capacity of 1.76 wt% within 50 cycles. Beom *et al.* [207] prepared the $Ti_{0.2}Zr_{0.2}Nb_{0.2}V_{0.2}Cr_{0.17}Fe_{0.03}$ HEA ingot with BCC and FCC dual-phase structure which was able to absorb hydrogen under 5 bar hydrogen pressure and room temperature without any thermal activation process. By studying the BCC phase ingots and FCC phase ingots with the corresponding compositions, it was found that the BCC phase did not react with hydrogen, and the FCC phase absorbed hydrogen. Further studies showed that the highly reactive oxide layer formed on the FCC ingot had a high Cr concentration, which might improve the reactivity of the oxide layer with hydrogen. Parisa *et al.* [208] designed a high-entropy TiZrCrMnFeNi alloy for hydrogen storage at room temperature based on the following three criteria: $VEC = 6.4$ (dehydrogenation can occur at room temperature if VEC is 6.4), single-phase thermodynamic stability (checked by CALPHAD calculations) and the formation of AB_2H_3 hydride (A: hydride-forming elements, B: elements with no affinity for hydrogen, H: hydrogen). The alloy contained 95 wt% C14 Laves phase, which absorbed and desorbed 1.7 wt% hydrogen at room temperature with rapid kinetics without activation treatment. Zhang *et al.* [209] prepared a TiZrNbTa HEA with single BCC solid solution phase, and found that many hydrides including ε-ZrH_2, ε-TiH_2 and β-(Nb, Ta)H were formed after hydrogenation. The TiZrNbTa alloy exhibited fast hydrogen absorption kinetics after a short incubation at room temperature, and the hydrogen absorption mechanism was determined to be nucleation and growth mechanism. The hydrogen absorption capacity at 293 K decreased slowly with cycling and maintained 86% after 10 cycles. Fukagawa *et al.* [210] developed a group of $Zr_{0.2}Ti_{0.2}Ni_{0.2+x}Cr_{0.2}Mn_{0.2}$ (x = 0 - 0.1) two-phase alloys with the main C14-type $(Zr_{0.5}Ti_{0.5})Mn_2$ phase and the secondary B2-type $Ti_{0.6}Zr_{0.4}Ni$ phase to overcome the difficulty in the hydrogen desorption under room temperature for HEAs. With the increase of Ni content, the secondary phase abundance increased, decreasing the stability of the hydrides. The $x = 0.075$ alloy obtained a discharge capacity of 368 $mAh \cdot g^{-1}$. Ma *et al.* [211]

found that partial substitution of Fe could be beneficial to improve the hydrogen storage capacity of HEAs and reduce the dehydrogenation temperature of the alloy hydrides. They prepared $ZrTiVAl_{1-x}Fe_x$ (x = 0 - 1) HEAs composed of C14-type Laves phase and HCP phase which exhibited fast hydrogen absorption kinetics at room temperature. With the increase of Fe content, the abundance of the C14-type Laves phase increased, which shortened the diffusion distance of H atoms and improved the hydrogenation kinetics. When Al was completely replaced by Fe, the ZrTiVFe alloy could absorb 1.58 wt% hydrogen even under 1 MPa H_2 pressure and room temperature. The increase of Fe content also increased the average VEC which decreased the stability of the alloy hydrides and thus reduced the hydrogen desorption temperature. Floriano *et al.* [212] compared the hydrogen storage properties of the equiatomic TiZrNbFeNi and nequiatomic $Ti_{20}Zr_{20}Nb_5Fe_{40}Ni_{15}$ HEAs. The alloys reached the maximum hydrogen storage capacity of 1.64 wt% and 1.38 wt%, respectively but the non-equiatomic alloy exhibited excellent hydrogen reversibility of 1.14 wt%. But the understanding and development of HEAs are still in its infancy.

7. Conclusions and Outlooks

New and efficient hydrogen storage materials and safe hydrogen storage technologies are urgently needed for the development and utilization of hydrogen energy. Therefore, the development of high-performance hydrogen storage alloys will still be an important direction for the future research. It can be seen from the present review that different types of hydrogen storage alloys have their own structure and hydrogen storage characteristics due to the different elemental components and preparation and subsequent modification methods. To ensure that the comprehensive properties of hydrogen storage alloys are suitable for practical applications, the diversification of elemental compositions and structures as well as the combination of preparation technologies will become the trend. Element substitution and catalyst doping are important methods. Among different types of hydrogen storage alloys, V-based solid solution alloys are the recent development direction for industrialization due to its high hydrogen storage capacity, low cost and mature technology, and Mg-based hydrogen storage alloys will become the long-term development direction. Further, it is also necessary to develop hydrogen storage alloys for different purposes by using model prediction based on calculated data. It is hoped that this review can enlighten novel ideas and methods for the reasonable design, rapid development and large-scale production of high-performance hydrogen storage alloys.

Acknowledgements

This work was financially supported by the project of the Inner Mongolia Autonomous Region (Nos. 2023JBGS0016), the Ordos major science and technology plan project (Nos. 2021EEDSCXQDFZ015) and the Rare Earth New Materials Technology Innovation Center "Directional selection".

Conflicts of Interest

The authors declare no conflicts of interest regarding the publication of this paper.

References

[1] Lu, X., Zhang, L., Yu, H., Lu, Z., He, J., Zheng, J., *et al.* (2021) Achieving Superior Hydrogen Storage Properties of MgH_2 by the Effect of TiFe and Carbon Nanotubes. *Chemical Engineering Journal*, **422**, Article ID: 130101. https://doi.org/10.1016/j.cej.2021.130101

[2] Ahmad, M.A.N., Sazelee, N., Ali, N.A. and Ismail, M. (2022) An Overview of the Recent Advances of Additive-Improved $Mg(BH_4)_2$ for Solid-State Hydrogen Storage Material. *Energies*, **15**, Article 862. https://doi.org/10.3390/en15030862

[3] Xia, Y., Yang, Z. and Zhu, Y. (2013) Porous Carbon-Based Materials for Hydrogen Storage: Advancement and Challenges. *Journal of Materials Chemistry A*, **1**, 9365-9381. https://doi.org/10.1039/c3ta10583k

[4] Zhao, D., Wang, X., Yue, L., He, Y. and Chen, B. (2022) Porous Metal-Organic Frameworks for Hydrogen Storage. *Chemical Communications*, **58**, 11059-11078. https://doi.org/10.1039/d2cc04036k

[5] El Kharbachi, A., Dematteis, E.M., Shinzato, K., Stevenson, S.C., Bannenberg, L.J., Heere, M., *et al.* (2020) Metal Hydrides and Related Materials. Energy Carriers for Novel Hydrogen and Electrochemical Storage. *The Journal of Physical Chemistry C*, **124**, 7599-7607. https://doi.org/10.1021/acs.jpcc.0c01806

[6] Ali, N.A. and Ismail, M. (2021) Modification of $NaAlH_4$ Properties Using Catalysts for Solid-State Hydrogen Storage: A Review. *International Journal of Hydrogen Energy*, **46**, 766-782. https://doi.org/10.1016/j.ijhydene.2020.10.011

[7] Sazelee, N.A. and Ismail, M. (2021) Recent Advances in Catalyst-Enhanced Lialh4 for Solid-State Hydrogen Storage: A Review. *International Journal of Hydrogen Energy*, **46**, 9123-9141. https://doi.org/10.1016/j.ijhydene.2020.12.208

[8] Ali, N.A., Sazelee, N.A. and Ismail, M. (2021) An Overview of Reactive Hydride Composite (RHC) for Solid-State Hydrogen Storage Materials. *International Journal of Hydrogen Energy*, **46**, 31674-31698. https://doi.org/10.1016/j.ijhydene.2021.07.058

[9] Jin, J., Yang, H.M., Quan, Y.W., Wang, W. and Wu, S.X. (2023) Research Progress in Carbon-Based Hydrogen Storage Materials Based on Physical Adsorption. *Coal Processing and Comprehensive Utilization*, **8**, 74.

[10] Liu, H.M., Xu, X.Y., Zhang, L.X., Wu, J.J. and Liu, D.B. (2021) Research Progress of Hydrogen Storage Technology. *Potrochemical Industry Technology*, **50**, 1101.

[11] Li, J.S., Ren, C.X., Luo, Z. and Chen, H.X. (2022) Technological Progress on the Research and Development of Solid Hydrogen Storage Materials. *Oil and Gas Energy*, **34**, 14.

[12] Tong, Y.H., Wang, J.Y., Hao, Z.Y., Liu, B.Q., Lin, W. and Su, L.Y. (2023) Review of the Development of Hydrogen Storage Technology in Space Propulsion. *Aerospace Technology*, **4**, 11.

[13] Wang, Y.X., Zhong, S.B. and Sun, F.C. (2022) Research Progress in Vehicular High Mass Density Solid Hydrogen Storage Materials. *Rare Metals*, **46**, 796.

[14] Kazakov, A.N., Bodikov, V.Y. and Blinov, D.V. (2021) Electrochemical Properties of Ab_5type $La_{0.8}Ce_{0.2}Ni_4Co_{0.5}Mn_{0.3}Al_{0.2}$ Alloy for Unified Metal Hydride Fuel Cell. *IOP Conference Series*: *Materials Science and Engineering*, **1035**, Article ID: 012016.

https://doi.org/10.1088/1757-899x/1035/1/012016

[15] Ma, T.X., Gao, L.Z., Hu, M.J., Hu, L.W., Wen, L.Y. and Hu, M.L. (2018) Research Progress of Solid Hydrogen Storage Materials. *Journal of Functional Materials*, **49**, 4001-4006.

[16] Zhang, X.F., Jiang, L.J., Ye, J.H., Wu,Y.F., Guo, X.M., Li, Z.N. and Li, H.W. (2022) Research Progress of Solid State Hydrogen Storage Technology. *Acta Energiae Solaris Sinica*, **43**, 345.

[17] Wang, L., Yan, H.Z. and Wu, J.M. (2018) Research and Development Status of Rare Earth Hydrogen Storage Alloys. *Rare Earths Statistics and Information*, **3**, 8.

[18] Yong, H., Li, Y.C., Hu, J.F., Gao, J.L. and Wang, S. (2021) Research Research of Mg-Based Hydrogen Storage Material. ***Metallic Functional Materials***, **28**, 50.

[19] Hu, L., Li, J.P., Zhao, X., Li, J.H. and Chen, J. (2018) Effect of Chemically Deposited Polypyrrole on Electrochemical Kinetic Properties of $LaNi_{3.81}Mn_{0.3}Co_{0.79}Al_{0.1}$ Hydrogen Storage Alloy. *Chinese Rare Metals*, **39**, 34-42.

[20] Li, Z., Li, S., Yuan, Z., Zhang, Y. and Qi, Y. (2019) Microstructure, Hydrogen Storage Thermodynamics and Kinetics of $La_5Mg_{95-x}Ni_x$ (x = 5, 10, 15) Alloys. *Transactions of Nonferrous Metals Society of China*, **29**, 1057-1066. https://doi.org/10.1016/s1003-6326(19)65014-4

[21] Hu, F., Luo, L.R., Li, Y.Z., Zhuo, T.T., Zhao, X. and Zhang, Y.H. (2019) Investigations in Electrochemical Thermodynamic and Kinetic Properties of AS-Cast and AS-Quenched $CeMg_{10}Ni_2$ Hydrogen Storage Alloys. *Journal of Electrochemistry*, **25**, 631-638.

[22] Zhu, M. and Ou, Y.L.Z. (2021) Kinetics Tuning and Electrochemical Performance of Mg-Based Hydrogen Storage Alloys. *Acta Metallurgica Sinica*, **57**, 1416.

[23] Fu, K.K., Zhao, X., Ke, D.D., Qi, Y.T., Hu, F., Cai, Y., Yan, H.P. and Duan, Y.N. (2023) Effect of Ce Sub-Stitution for La on the Hydrogen Storage Properties and Thermodynamics of Alloy $LaNi_{4.5}Al_{0.5}$. *Chinese Rare Earths*, **44**, 86.

[24] Zeng, L.Y., Zhang, S.Y., Li, Q., Qi, Y.L., Li, S.L., Xin, S.W., Mao, C.L., Zhang, B.J. and Cai, J.H. (2022) Research Progress on Ti-Based Hydrogen Storage Alloy. *Ti Industry Progress*, **39**, 39.

[25] Xu, W., Tao, Z.L. and Chen, J. (2006) Progress of Research on Hydrogen Storage. *Progress in Chemistry*, **18**, 200.

[26] Yang, C.Z. (2020) The Characters and Mechanism Research of Hydrogen Absorption/Desorption Kinetics for Alloy Hydrogen Storage Materials. *Material Sciences*, **10**, 1002-1026. https://doi.org/10.12677/ms.2020.1012120

[27] Li, Q. (2022) Review on the Development of Rare Earth Hydrogen Storage Materials. *Rare Earth Infor*mation, **3**, 36.

[28] Li, Y., Zhang, L. and Han, S.M. (2020) Rare Earth—Mg-Ni Superlattice Alloy Structure Research and Progress on Hydrogen Storage Properties. *Journal of Yanshan University*, **44**, 323.

[29] Ouyang, L., Huang, J., Wang, H., Liu, J. and Zhu, M. (2017) Progress of Hydrogen Storage Alloys for Ni-Mh Rechargeable Power Batteries in Electric Vehicles: A Review. *Materials Chemistry and Physics*, **200**, 164-178. https://doi.org/10.1016/j.matchemphys.2017.07.002

[30] Tan, C., Ouyang, L., Wang, H., Min, D., Liao, C., Xiao, F., *et al.* (2020) Effect of Y Substitution on the High Rate Dischargeability of $AB_{4.6}$ Alloys as an Electrode Material for Nickel Metal Hydride Batteries. *Journal of Alloys and Compounds*, **849**, Article ID: 156641. https://doi.org/10.1016/j.jallcom.2020.156641

[31] Kazakov, A.N., Blinov, D.V., Bodikov, V.Y., Mitrokhin, S.V. and Volodin, A.A. (2021) Hydrogen Storage and Electrochemical Properties of Annealed Low-Co AB_5 Type Intermetallic Compounds. *International Journal of Hydrogen Energy*, **46**, 13622-13631. https://doi.org/10.1016/j.ijhydene.2020.12.071

[32] Han, X., Wu, W., Bian, X., Liu, X., Huang, L. and Wu, J. (2016) A Performance Study of AB_5 Hydrogen Storage Alloys with Co Being Replaced by Be-Cu. *International Journal of Hydrogen Energy*, **41**, 7445-7452. https://doi.org/10.1016/j.ijhydene.2016.03.100

[33] Chen, X., Xu, J., Zhang, W., Zhu, S., Zhang, N., Ke, D., *et al.* (2021) Effect of Mn on the Long-Term Cycling Performance of AB_5-Type Hydrogen Storage Alloy. *International Journal of Hydrogen Energy*, **46**, 21973-21983. https://doi.org/10.1016/j.ijhydene.2021.04.021

[34] Zhou, W., Zhu, D., Tang, Z., Wu, C., Huang, L., Ma, Z., *et al.* (2017) Improvement in Low-Temperature and Instantaneous High-Rate Output Performance of Al-Free AB_5-Type Hydrogen Storage Alloy for Negative Electrode in Ni/MH Battery: Effect of Thermodynamic and Kinetic Regulation via Partial Mn Substituting. *Journal of Power Sources*, **343**, 11-21. https://doi.org/10.1016/j.jpowsour.2017.01.023

[35] Xu, J., Chen, X., Zhu, W., Zhang, W., Cui, H., Zhu, S., *et al.* (2022) Enhanced Cycling Stability and Reduced Hysteresis of AB_5-Type Hydrogen Storage Alloys by Partial Substitution of Sn for Ni. *International Journal of Hydrogen Energy*, **47**, 22495-22509. https://doi.org/10.1016/j.ijhydene.2022.05.071

[36] Zhou, W., Zhu, D., Liu, K., Li, J., Wu, C. and Chen, Y. (2018) Long-Life Ni-MH Batteries with High-Power Delivery at Lower Temperatures: Coordination of Low-Temperature and High-Power Delivery with Cycling Life of Low-Al AB_5-Type Hydrogen Storage Alloys. *International Journal of Hydrogen Energy*, **43**, 21464-21477. https://doi.org/10.1016/j.ijhydene.2018.09.166

[37] Chen, M., Tan, C., Jiang, W., Huang, J., Min, D., Liao, C., *et al.* (2021) Influence of Over-Stoichiometry on Hydrogen Storage and Electrochemical Properties of Sm-Doped Low-Co AB_5-Type Alloys as Negative Electrode Materials in Nickel-Metal Hydride Batteries. *Journal of Alloys and Compounds*, **867**, Article ID: 159111. https://doi.org/10.1016/j.jallcom.2021.159111

[38] Panwar, K. and Srivastava, S. (2019) On Structural Model of AB_5-Type Multi-Element Hydrogen Storage Alloy. *International Journal of Hydrogen Energy*, **44**, 30208-30217. https://doi.org/10.1016/j.ijhydene.2019.09.138

[39] Yao, Q., Tang, Y., Zhou, H., Deng, J., Wang, Z., Pan, S., *et al.* (2014) Effect of Rapid Solidification Treatment on Structure and Electrochemical Performance of Low-Co AB_5-Type Hydrogen Storage Alloy. *Journal of Rare Earths*, **32**, 526-531. https://doi.org/10.1016/s1002-0721(14)60103-4

[40] Zhu, X.M., Liu, Z.P., Wang, Y.G., Jing, Y.Q., Luo, T.Z., Li, Q. and Xu, Y.Y. (2022) Study on Annealing Process of $MlNi_{4.57}Co_{0.17}Mn_{0.25}Al_{0.41}Y_{0.02}$ Low Co and Long Life Hydrogen Storage Alloy. *Hot Working Technology*, **53**, 46-50.

[41] Lv, L.J., Lin, J., Yang, G., Ma, Z.W., *et al.* (2022) Hydrogen Storage Performance of $LaNi_{3.95}Al_{0.75}Co_{0.3}$ Alloy with Different Preparation Methods. *Progress in Natural Science-Materials International*, **32**, 206-214. https://doi.org/10.1016/j.pnsc.2022.02.001

[42] Gan, H.H., Yang, Y.F. and Shao, H.X. (2015) High Rate Performance of $MINi_{4.07}Co_{0.45}Mn_{0.38}Al_{0.31}$ Hydrogen Storage Alloy. *Battery Bimonthly*, **45**, 194.

[43] Hubkowska, K., Soszko, M., Krajewski, M. and Czerwiński, A. (2019) Enhanced Kinetics of Hydrogen Electrosorption in AB_5 Hydrogen Storage Alloy Decorated with

Pd Nanoparticles. *Electrochemistry Communications*, **100**, 100-103. https://doi.org/10.1016/j.elecom.2019.02.007

[44] Zhu, S., Chen, X., Liu, J., Yang, N., Chen, J., Gu, C., *et al.* (2020) Long-term Hydrogen Absorption/desorption Properties of an AB_5-Type $LaNi_{4.75}Mn_{0.25}$ Alloy. *Materials Science and Engineering*: *B*, **262**, Article ID: 114777. https://doi.org/10.1016/j.mseb.2020.114777

[45] Nowak, M., Balcerzak, M. and Jurczyk, M. (2018) Hydrogen Storage and Electrochemical Properties of Mechanically Alloyed $La_{1.5-x}Gd_xMg_{0.5}Ni_7$ ($0 \le x \le 1.5$). *International Journal of Hydrogen Energy*, **43**, 8897-8906. https://doi.org/10.1016/j.ijhydene.2018.03.130

[46] Ma, Y.R., Dong, X.P., Chen, Y.F., Ran, T., Li, Z.Y., Li, H.D. and Su, D.D. (2020) Capacity Attenuation and Microstructure of La-Mg-Ni Hydrogen Storage Alloys. *Engineering Science and Technology*, **20**, Article ID: 10214.

[47] Chen, Y., Mo, X., Huang, Y., Hu, C., Zuo, X., Wei, Q., *et al.* (2022) The Role of Magnesium on Properties of $La_{3-X}Mg_xNi_9$ (x = 0, 0.5, 1.0, 1.5, 2.0) Hydrogen Storage Alloys from First-Principles Calculations. *International Journal of Hydrogen Energy*, **47**, 36408-36417. https://doi.org/10.1016/j.ijhydene.2022.08.242

[48] Wang, B., Wang, Y., Xue, T., Zou, Z. and Liu, Z. (2021) The Morphology and Electrochemical Properties of $La_{1-x}Mg_xNi_{3.4}Al_{0.1}$ (x = 0.1 – 0.4) Hydrogen Storage Alloys. *International Journal of Hydrogen Energy*, **46**, 35653-35661. https://doi.org/10.1016/j.ijhydene.2021.08.114

[49] Dong, Z.W., Zhang, S.Y., Ma, R.B., Wu, X.W. and Gao, Y.H. (2018) Preparation and Electrochemical Hydrogenation Properties of $La_{1-x}Mg_xNi_{2.5}Co_{0.5}$ (x = 0~0.4) Hydrogen Storage Alloys. *Journal of Material Sciences & Engineering*, **36**, 573.

[50] Zhou, N., Du, W., Zhang, P., Zhu, Y., Wang, Z., Liu, K., *et al.* (2016) Microstructure and Electrochemical Properties of $La_{0.8-x}$ $MM_XMg_{0.2}Ni_{3.1}Co_{0.3}Al_{0.1}$ (x = 0, 0.1, 0.2, 0.3) Alloys. *Rare Metals*, **36**, 645-650. https://doi.org/10.1007/s12598-016-0716-5

[51] Xu, J.F., Zhang, G.F., Hu, F., Wang, R.F., Dou, Y. and Zhang, Y. (2020) Phase Structure and Electro-Chemical Performance for Super Lattice La-Mg-Ni Based A_5B_{19} Type Negative Materials. *Journal of Materials and Engineering*, **48**, 46.

[52] Huang, X.T., Lu, Z., Qing, P.L. and Tan, C.S. (2016) Study on the Hydrogen Properties and Electro-Chemical Performance of $La_{0.7-x}Pr_xZr_{0.1}Mg_{0.2}Ni_{2.75}Co_{0.45}Fe_{0.1}Al_{0.2}$(x = 0, 0.05, 0.10, 0.15, 0.20) Alloys. *Materials Reports*, **30**, 33.

[53] Liu, J., Chen, X., Xu, J., Zhu, S., Cheng, H., Yang, G., *et al.* (2021) A New Strategy for Enhancing the Cycling Stability of Superlattice Hydrogen Storage Alloys. *Chemical Engineering Journal*, **418**, Article ID: 129395. https://doi.org/10.1016/j.cej.2021.129395

[54] Li, Y.M., Liu, Z.C., Zhang, Y.H. and Ren, H.P. (2019) The Effect of Zn Substitution on the Phase Structure of AB3 La-Mg-Ni Alloy Influence of Electrochemical Properties and Failure Behavior. Chinese. *The Chinese Journal of Nonferrous Metals*, **29**, 1028.

[55] Wang, W., Xu, G., Zhang, L., Ma, C., Zhao, Y., Zhang, H., *et al.* (2021) Electrochemical Features of Ce_2Ni_7-Type $La_{0.65}Nd_{0.15}Mg_{0.25}Ni_{3.20}M_{0.10}$ (M = Ni, Mn and Al) Hydrogen Storage Alloys for Rechargeable Nickel Metal Hydride Battery. *Journal of Alloys and Compounds*, **861**, Article ID: 158469. https://doi.org/10.1016/j.jallcom.2020.158469

[56] Fan, Y., Zhang, L., Xue, C., Fan, G., Liu, J., Liu, B., *et al.* (2019) Superior Electrochemical Performances of La-Mg-Ni Alloys with A_2B_7/A_5B_{19} Double Phase. *International Journal of Hydrogen Energy*, **44**, 7402-7413.

https://doi.org/10.1016/j.ijhydene.2019.01.188

[57] Zhang, Y., Gong, P., Li, L., Sun, H., Feng, D. and Guo, S. (2017) Hydrogen Storage Thermodynamics and Dynamics of La-Mg-Ni-Based $LaMg_{12}$-Type Alloys Synthesized by Mechanical Milling. *Rare Metals*, **38**, 1144-1152. https://doi.org/10.1007/s12598-016-0842-0

[58] Zhang, H., Fu, L., Xuan, W. and Qi, J. (2020) Surface Modification of the $La_{1.7}Mg_{1.3}Ni_9$ Alloy with Trace Y_2O_3 Related to the Electrochemical Hydrogen Storage Properties. *Renewable Energy*, **145**, 1572-1577. https://doi.org/10.1016/j.renene.2019.07.080

[59] Luo, L.R., Cai, Y. and Hu, F. (2019) Electrochemical and Kinetic Properties of As-Cast and Quenched $CeMg_{11}Ni$ Hydrogen Storage Alloys. *Energy Storage Science and Technology*, **8**, 904-910.

[60] Li, Y., An, X., Liu, Z., Zhang, Y. and Ren, H. (2019) Microstructural Heredity of the La Mg Ni Based Electrode Alloys during Annealing. *International Journal of Hydrogen Energy*, **44**, 29344-29355. https://doi.org/10.1016/j.ijhydene.2019.01.179

[61] Chen, Y.F., Dong, X.P., Ma, Y.R., Li, X., Gao, T.Y. and Su, J.W. (2020) Effect of Annealing Time on Structure and Gaseous Hydrogen Absorption and Desorption Properties of $LaMgNi_{3.9}Mn_{0.2}$ Alloy. *Rare Hard Metals*, **48**, 904.

[62] Deng, A.Q., Luo, Y.C., Wang, H., Zhao, L. and Luo, Y.W. (2018) Effect of Annealing Treatment on the Phase Structure and Electrochemical Properties of $La_{0.63}(Pr_{0.1}Nd_{0.1}Y_{0.6}Sm_{0.1}Gd_{0.1})_{0.2}Mg_{0.17}Ni_{3.1}Co_{0.3}Al_{0.1}A_2B_7$-Type Hydrogen Storage Alloys. *Materials Reports*, **32**, 2565.

[63] Jiao, Q.T., Pan, W., Zhu, S., Chen, X.Y., Yang, N., Chen, J., Gu, C.N., Qiu, T. and Liu, J.J. (2021) Effects of Phase Composition on Electrochemical Properties of $La_{0.75}Mg_{0.25}Ni_{3.5}$ Hydrogen Storage Alloy. *Materials Reports*, **35**, 6140.

[64] Young, K., Ouchi, T. and Huang, B. (2014) Effects of Various Annealing Conditions on (Nd, Mg, Zr) $(Ni, Al, Co)_{3.74}$ Metal Hydride Alloys. *Journal of Power Sources*, **248**, 147-153. https://doi.org/10.1016/j.jpowsour.2013.09.037

[65] He, X., Xiong, W., Wang, L., Li, B., Li, J., Zhou, S., *et al.* (2022) Study on the Evolution of Phase and Properties for Ternary La-Y-Ni-Based Hydrogen Storage Alloys with Different Stoichiometric Ratios. *Journal of Alloys and Compounds*, **921**, Article ID: 166064. https://doi.org/10.1016/j.jallcom.2022.166064

[66] Yan, H., Xiong, W., Wang, L., Li, B., Li, J. and Zhao, X. (2017) Investigations on AB_3-, A_2B_7- and A_5B_{19}-Type La Y Ni System Hydrogen Storage Alloys. *International Journal of Hydrogen Energy*, **42**, 2257-2264. https://doi.org/10.1016/j.ijhydene.2016.09.049

[67] Zhao, L., Luo, Y.C., Deng, A.Q. and Jiang, W.T. (2018) Mg-Free Superlattice Structure $A_2B_7La_{1-x}Y_xNi_{3.25}Mn_{0.15}Al_{0.1}$ Hydrogen Storage and Electrochemical Properties of Alloys. *Chemical Journal of Chinese Universities*, **39**, 1993.

[68] Liu, Y., Yuan, H., Guo, M. and Jiang, L. (2019) Effect of Y Element on Cyclic Stability of A_2B_7-Type La-Y-Ni-Based Hydrogen Storage Alloy. *International Journal of Hydrogen Energy*, **44**, 22064-22073. https://doi.org/10.1016/j.ijhydene.2019.06.081

[69] Guo, Y., Shi, Y., Yuan, R., Leng, H. and Li, Q. (2021) Inhibition Mechanism of Capacity Degradation in Mg-Substituted $LaY_{2-x}Mg_xNi_9$ Hydrogen Storage Alloys. *Journal of Alloys and Compounds*, **873**, Article ID: 159826. https://doi.org/10.1016/j.jallcom.2021.159826

[70] Zhao, L.Q., Deng, A.Q., Yang, Y., Kang, X.Y. and Luo, Y.C. (2022) Study on Phase Structure, Hydrogen Storage and Electrochemical Properties of La-Nd-Y-Ni A_5B_{19} Annealed Alloy. *Journal of the Chinese Society of Rare Earths*, **40**, 250.

[71] Guo, M., Yuan, H., Liu, Y. and Jiang, L. (2021) Effect of SM on the Cyclic Stability of

La-Y-Ni-Based Alloys and Their Comparison with Re-Mg-Ni-Based Hydrogen Storage Alloy. *International Journal of Hydrogen Energy*, **46**, 7432-7441. https://doi.org/10.1016/j.ijhydene.2020.11.195

[72] Yang, Y., Luo, Y.C., Mei, X.Z., Wang, H. and Deng, A.Q. (2017) Microstructure and Electrochemical Properties of A_2B_7 $La_{0.63}$(Pr, Nd, Y, Sm, Gd)$_{0.2}Mg_{0.17}Ni_{3.1}Co_{0.3}Al_{0.1}$ Hydrogen Storage Alloy. *Journal of Functional Materials*, **48**, 8135-8141.

[73] Wang, L., Zhang, X., Zhou, S., Xu, J., Yan, H., Luo, Q., *et al.* (2020) Effect of Al Content on the Structural and Electrochemical Properties of A_2B_7 Type La-Y-Ni Based Hydrogen Storage Alloy. *International Journal of Hydrogen Energy*, **45**, 16677-16689. https://doi.org/10.1016/j.ijhydene.2020.04.136

[74] Xiong, W., Yan, H., Wang, L., Verbetsky, V., Zhao, X., Mitrokhin, S., *et al.* (2017) Characteristics of A_2B_7-Type La Y Ni-Based Hydrogen Storage Alloys Modified by Partially Substituting Ni with Mn. *International Journal of Hydrogen Energy*, **42**, 10131-10141. https://doi.org/10.1016/j.ijhydene.2017.01.080

[75] Zhou, S.J., Zhang, X., Xu, J., Zhao, Y.Y. and Yan, H.Z. (2022) Study on Element Regulation and Low Temperature Characteristics of a New La-Y-Ni Hydrogen Storage Alloy. *Journal of the Chinese Society of Rare Earths*, **40**, 805.

[76] Wang, H., Luo, Y.C., Deng, A.Q., Zhao, L. and Jiang, W.T. (2018) Effect of Annealing Temperature on Phase Structure and Electrochemical Properties of La-Y-Ni A_2B_7 Alloy without Mg. *Journal of Inorganic Materials*, **33**, 434.

[77] Li, J.P., Deng, A.Q., Yang, Y., Pan, F.J., Zhang, H.M. and Luo, Y.C. (2022) Phase Structure and Electro-Chemical Properties of La-Y-Ni A_5B_{19} Annealed Alloy. *The Chinese Journal of Nonferrous Metals*, **32**, 788.

[78] Guo, M., Yuan, H.P., Liu, Y.R. and Jiang, L.J. (2019) Effect of Heat Treatment Temperature on Phase Structure and Electrochemical Properties of La-Y-Ni Alloy. *Chinese Journal of Inorganic Chemistry*, **35**, 1041.

[79] Li, T., Luo, X.Y. and Chen, Z.R. (2022) Effect of Annealing Temperature on Electrochemical Properties of Hydrogen Storage Alloys for Automobile Nickel Metal Hydride Batteries. *Chinese Rare Earths*, **43**, 93.

[80] Zhou, S., Wang, L., Xiong, W., Li, B., Li, J., Zhang, X., *et al.* (2022) High Temperature Phase Transformation and Low Temperature Electrochemical Properties of $La_{1.9}Y_{4.1}Ni_{20.8}Mn_{0.2}Al$ H_2-Storage Alloy. *International Journal of Hydrogen Energy*, **47**, 2547-2560. https://doi.org/10.1016/j.ijhydene.2021.10.188

[81] Zhao, S., Wang, H., Hu, R., Jiang, W., Liu, J., Ouyang, L., *et al.* (2021) Phase Transformation and Hydrogen Storage Properties of $Lay_2Ni_{10.5}$ Superlattice Alloy with Single Gd_2Co_7-Type or Ce_2Ni_7-Type Structure. *Journal of Alloys and Compounds*, **868**, Article ID: 159254. https://doi.org/10.1016/j.jallcom.2021.159254

[82] Zhao, S., Yang, L., Liu, J., Ouyang, L., Zhu, M. and Wang, H. (2022) Structural Evolution and Electrochemical Hydrogen Storage Properties of Single-Phase A_5B_{19}-Type $(La_{0.33}Y_{0.67})_5Ni_{17.6}Mn_{0.9}Al_{0.5}$ Alloy. *Journal of Power Sources*, **548**, Article ID: 232039. https://doi.org/10.1016/j.jpowsour.2022.232039

[83] Xing, L., Li, Y.M., Zhang, Y.H., Ren, H.P. and Jin, Z.L. (2017) Electrochemical Hydrogen Storage Properties and Failure Behavior of Fast Quenched and Annealed La_4MgNi_{19} Alloy. *Chinese Journal of Rare Metals*, **41**, 1318.

[84] Wu, R., Yuan, H., Liu, Y., Hou, Z., Li, Z., Wang, S., *et al.* (2022) Effect of Carbon Coating on Electrochemical Properties of $AB_{3.5}$-Type La-Y-Ni-Based Hydrogen Storage Alloys. *Journal of Rare Earths*, **40**, 1264-1271. https://doi.org/10.1016/j.jre.2021.06.005

[85] Ali, N.A. and Ismail, M. (2021) Advanced Hydrogen Storage of the Mg-Na-Al System: A Review. *Journal of Magnesium and Alloys*, **9**, 1111-1122. https://doi.org/10.1016/j.jma.2021.03.031

[86] Wei, Z., Feng, D.C., Zhai, T.T., Yuan, Z.M. and Zhang, Y.H. (2021) Electrochemical Performance of $La_{2-x}Sm_xMg_{16}Ni$ (x = 0.1-0.4) + 100%Ni + 5%Graphene Composite Hydrogen Storage Alloys. *Metallic Functional Materials*, **29**, 33-39.

[87] Li, B., Li, J., Zhao, H., Yu, X. and Shao, H. (2019) Mg-Based Metastable Nano Alloys for Hydrogen Storage. *International Journal of Hydrogen Energy*, **44**, 6007-6018. https://doi.org/10.1016/j.ijhydene.2019.01.127

[88] Li, Y., Yang, J., Luo, L., Hu, F., Zhai, T., Zhao, Z., *et al.* (2019) Microstructure Characteristics, Hydrogen Storage Kinetic and Thermodynamic Properties of Mg_{80}-NiY (x = 0 – 7) Alloys. *International Journal of Hydrogen Energy*, **44**, 7371-7380. https://doi.org/10.1016/j.ijhydene.2019.01.216

[89] Zhang, W., Zhao, D., Zhang, Y., Li, J., Guo, S., Qi, Y., *et al.* (2022) Effect of Y Partially Substituting La on the Phase Structure and Hydrogen Storage Property of La-Mg-Ni Alloys. *Journal of Physics and Chemistry of Solids*, **167**, Article ID: 110744. https://doi.org/10.1016/j.jpcs.2022.110744

[90] Gao, J.L., Shang, H.W., Li, Y.Q., Yuan, Z.M., Zhao, D.L. and Zhang, Y.H. (2017) Gaseous Hydrogen Storage Kinetics of La-Mg-Ni-Cu Series Mg_2Ni Alloy. *The Chinese Journal of Nonferrous Metals*, **27**, 1132.

[91] Kang, H., Yong, H., Wang, J., Xu, S., Li, L., Wang, S., *et al.* (2021) Characterization on the Kinetics and Thermodynamics of Mg-Based Hydrogen Storage Alloy by the Multiple Alloying of Ce, Ni and Y Elements. *Materials Characterization*, **182**, Article ID: 111583. https://doi.org/10.1016/j.matchar.2021.111583

[92] Yong, H., Guo, S., Yuan, Z., Qi, Y., Zhao, D. and Zhang, Y. (2020) Catalytic Effect of in Situ Formed Mg_2Ni and REH (RE: Ce and Y) on Thermodynamics and Kinetics of Mg-Re-Ni Hydrogen Storage Alloy. *Renewable Energy*, **157**, 828-839. https://doi.org/10.1016/j.renene.2020.05.043

[93] Sun, H., Zhao, F.G., Feng, X.C., Ren, H.P. and Zhang, Y.H. (2020) Activation and Hydrogen Absorption Properties of $Mg_{22}Y_2Ni_{10}Cu_2$ Hydrogen Storage Alloy. *Chinese Journal of Rare Metals*, **44**, 387.

[94] Zhang, Y., Sun, H., Zhang, W., Wei, X., Yuan, Z., Gao, J., *et al.* (2021) A Comparison Study of Hydrogen Storage Performances of As-Cast La_{10}-Re $Mg_{80}Ni_{10}$ (x = 0 or 3; RE = Sm or Ce) Alloys. *Journal of Alloys and Compounds*, **884**, Article ID: 160905. https://doi.org/10.1016/j.jallcom.2021.160905

[95] Zhong, H., Xu, J., Jiang, C. and Lu, X. (2018) Microstructure and Remarkably Improved Hydrogen Storage Properties of Mg_2Ni Alloys Doped with Metal Elements of Al, Mn and Ti. *Transactions of Nonferrous Metals Society of China*, **28**, 2470-2477. https://doi.org/10.1016/s1003-6326(18)64893-9

[96] Chen, L., Hu, C. and Liu, F. (2019) Microstructure and Hydrogen Storage Kinetics of $Mg_{89}Re_{11}$ (RE = Pr, Nd, Sm) Binary Alloys. *RSC Advances*, **9**, 4445-4452. https://doi.org/10.1039/c8ra08983c

[97] Cao, W., Ding, X., Zhang, Y., Zhang, J., Chen, R., Su, Y., *et al.* (2022) Formation of AlNi Phase and Its Influence on Hydrogen Absorption Kinetics of $Mg_{77}ni_{23}$-Al Alloys at Intermediate Temperatures. *International Journal of Hydrogen Energy*, **47**, 25733-25744. https://doi.org/10.1016/j.ijhydene.2022.06.022

[98] Yong, H., Wei, X., Wang, Y., Guo, S., Yuan, Z., Qi, Y., *et al.* (2020) Phase Evolution, Thermodynamics and Kinetics Property of Transition Metal (TM = Zr, Ti, V) Catalyzed Mg-Ce-Y-Ni Hydrogen Storage Alloys. *Journal of Physics and Chemistry of*

Solids, **144**, Article ID: 109516. https://doi.org/10.1016/j.jpcs.2020.109516

[99] Chen, Y., Zhang, H., Wu, F., Sun, Z., Zheng, J., Zhang, L., *et al.* (2021) Mn Nanoparticles Enhanced Dehydrogenation and Hydrogenation Kinetics of MgH_2 for Hydrogen Storage. *Transactions of Nonferrous Metals Society of China*, **31**, 3469-3477. https://doi.org/10.1016/s1003-6326(21)65743-6

[100] Zhang, J., Liu, H., Sun, P., Zhou, C., Guo, X. and Fang, Z.Z. (2023) The Role of Oxide in Hydrogen Absorption and Desorption Kinetics of MgH_2-Based Material. *Journal of Alloys and Compounds*, **934**, Article ID: 167757. https://doi.org/10.1016/j.jallcom.2022.167757

[101] Tian, G., Wu, F., Zhang, H., Wei, J., Zhao, H. and Zhang, L. (2023) Boosting the Hydrogen Storage Performance of MgH_2 by Vanadium Based Complex Oxides. *Journal of Physics and Chemistry of Solids*, **174**, Article ID: 111187. https://doi.org/10.1016/j.jpcs.2022.111187

[102] Wang, X., Xiao, X., Liang, Z., Zhang, S., Qi, J., Lv, L., *et al.* (2022) Ultrahigh Reversible Hydrogen Capacity and Synergetic Mechanism of $2LiBH_4$-MgH_2 System Catalyzed by Dual-Metal Fluoride. *Chemical Engineering Journal*, **433**, Article ID: 134482. https://doi.org/10.1016/j.cej.2021.134482

[103] Yong, H., Guo, S., Yuan, Z., Zhang, W., Qi, Y., Zhao, D., *et al.* (2020) Phase Evolution, Hydrogen Storage Thermodynamics and Kinetics of Ternary $Mg_{90}Ce_5Sm_5$ Alloy. *Journal of Rare Earths*, **38**, 633-641. https://doi.org/10.1016/j.jre.2019.05.012

[104] Jiang, M., Xu, J., Munroe, P. and Xie, Z. (2023) First-Principles Study on the Hydrogen Storage Properties of Mgh_2(101) Surface by CuNi Co-Doping. *Chemical Physics*, **565**, Article ID: 111760. https://doi.org/10.1016/j.chemphys.2022.111760

[105] Shang, Y., Jin, O., Puszkiel, J.A., Karimi, F., Dansirima, P., Sittiwet, C., *et al.* (2022) Effects of Metal-Based Additives on Dehydrogenation Process of $2NaBH_4 + MgH_2$ System. *International Journal of Hydrogen Energy*, **47**, 37882-37894. https://doi.org/10.1016/j.ijhydene.2022.08.293

[106] Liu, Z., Liu, J., Wu, Z., Tang, Q., Zhu, Y., Zhang, J., *et al.* (2022) Enhanced Hydrogen Sorption Kinetics of MgH_2 Catalyzed by a Novel Layered Ni/Al_2O_3 Hybrid. *Journal of Alloys and Compounds*, **895**, Article ID: 162682. https://doi.org/10.1016/j.jallcom.2021.162682

[107] Hou, Q., Zhang, J., Guo, X.T., Xu, G. and Yang, X. (2022) Synthesis of Low-Cost Biomass Charcoal-Based Ni Nanocatalyst and Evaluation of Their Kinetic Enhancement of MgH_2. *International Journal of Hydrogen Energy*, **47**, 15209-15223. https://doi.org/10.1016/j.ijhydene.2022.03.040

[108] Tome, K.C., Xi, S., Fu, Y., Lu, C., Lu, N., Guan, M., *et al.* (2022) Remarkable Catalytic Effect of Ni and ZrO_2 Nanoparticles on the Hydrogen Sorption Properties of MgH_2. *International Journal of Hydrogen Energy*, **47**, 4716-4724. https://doi.org/10.1016/j.ijhydene.2021.11.102

[109] Yu, Z., Zhang, W., Zhang, Y., Fu, Y., Cheng, Y., Guo, S., *et al.* (2022) Remarkable Kinetics of Novel $Ni@CeO_2$-MgH_2 Hydrogen Storage Composite. *International Journal of Hydrogen Energy*, **47**, 35352-35364. https://doi.org/10.1016/j.ijhydene.2022.08.121

[110] Ren, S., Fu, Y., Zhang, L., Cong, L., Xie, Y., Yu, H., *et al.* (2022) An Improved Hydrogen Storage Performance of MgH_2 Enabled by Core-Shell Structure Ni/Fe_3O_4@mil. *Journal of Alloys and Compounds*, **892**, Article ID: 162048. https://doi.org/10.1016/j.jallcom.2021.162048

[111] Song, Y.B. and Zhao, X. (2020) Preparation and properties of Mg_2Ni-Based Hydrogen Storage Al-oy for New Energy Vehicle. *Chinese Journal of Power Sources*, **44**, 186.

[112] Meena, P., Meena, A., Jangir, M., Sharma, V.K. and Jain, I.P. (2019) Mg-Based Nanocomposites for Hydrogen Storage Containing $La_{23}Nd_{8.5}Ti_{1.1}Ni_{33.9}Co_{32.9}Al_{0.65}$ Alloys as Additives. *Materials Today*: *Proceedings*, **18**, 901-911. https://doi.org/10.1016/j.matpr.2019.06.523

[113] Zaluski, L., Zaluska, A. and Ström-Olsen, J.O. (1995) Hydrogen Absorption in Nanocrystalline Mg_2Ni Formed by Mechanical Alloying. *Journal of Alloys and Compounds*, **217**, 245-249. https://doi.org/10.1016/0925-8388(94)01348-9

[114] Zhang, J., Liu, H., Sun, P., Guo, X., Zhou, C. and Fang, Z.Z. (2022) The Effects of Crystalline Defects on Hydrogen Absorption Kinetics of Catalyzed MgH_2 at Ambient Conditions. *Journal of Alloys and Compounds*, **927**, Article ID: 167090. https://doi.org/10.1016/j.jallcom.2022.167090

[115] Wen, J., de Rango, P., Allain, N., Laversenne, L. and Grosdidier, T. (2020) Improving Hydrogen Storage Performance of Mg-Based Alloy through Microstructure Optimization. *Journal of Power Sources*, **480**, Article ID: 228823. https://doi.org/10.1016/j.jpowsour.2020.228823

[116] Chen, J.N., Zhang, J., He, J.H., Zhou, X.J., Lu, X.Z., Chen, X.M., *et al.* (2022) A Comparative Study on Hydrogen Storage Properties of As-Cast and Extruded Mg-4.7Y-4.1Nd-0.5Zr Alloys. *Journal of Physics and Chemistry of Solids*, **161**, Article ID: 110483. https://doi.org/10.1016/j.jpcs.2021.110483

[117] Hu, Z.L. (2002) Hydrogen Storage Material. Chemical Industry Press.

[118] Solonin, Y.M., Galiy, O.Z., Karpets, M.V., Savenko, O.F., Shcherbakova, L.G., Schur, D.V., *et al.* (2022) Electrochemical Properties of the ZrNiMnCrV Alloy Depending on Quantitative Phase Composition. *Powder Metallurgy and Metal Ceramics*, **61**, 370-376. https://doi.org/10.1007/s11106-022-00323-8

[119] Yartys, V.A. and Lototskyy, M.V. (2022) Laves Type Intermetallic Compounds as Hydrogen Storage Materials: A Review. *Journal of Alloys and Compounds*, **916**, Article ID: 165219. https://doi.org/10.1016/j.jallcom.2022.165219

[120] Matsuyama, A., Mizutani, H., Kozuka, T. and Inoue, H. (2017) Effect of Ti Substitution on Electrochemical Properties of ZrNi Alloy Electrode for Use in Nickel-Metal Hydride Batteries. *International Journal of Hydrogen Energy*, **42**, 22622-22627. https://doi.org/10.1016/j.ijhydene.2017.03.119

[121] Wan, C., Denys, R.V. and Yartys, V.A. (2021) Effects of Ti Substitution for Zr on the Electrochemical Characteristics and Structure of AB_2-Type Laves-Phase Alloys as Metal Hydride Anodes. *Journal of Alloys and Compounds*, **889**, Article ID: 161655. https://doi.org/10.1016/j.jallcom.2021.161655

[122] Wan, C., Denys, R.V., Lelis, M., Milčius, D. and Yartys, V.A. (2019) Electrochemical Studies and Phase-Structural Characterization of a High-Capacity La-Doped AB_2 Laves Type Alloy and Its Hydride. *Journal of Power Sources*, **418**, 193-201. https://doi.org/10.1016/j.jpowsour.2019.02.044

[123] Leng, H., Yan, P., Han, X., Liu, W., Liu, Q. and Li, Q. (2020) Microstructural Characterization and Hydrogenation Performance of $ZrxV_5Fe$ (x = 3 - 9) Alloys. *Progress in Natural Science*: *Materials International*, **30**, 229-238. https://doi.org/10.1016/j.pnsc.2020.01.002

[124] Yao, Z., Xiao, X., Liang, Z., Huang, X., Kou, H., Luo, W., *et al.* (2019) Study on the Modification of Zr-Mn-V Based Alloys for Hydrogen Isotopes Storage and Delivery. *Journal of Alloys and Compounds*, **797**, 185-193. https://doi.org/10.1016/j.jallcom.2019.05.076

[125] Wu, Y., Peng, Y., Jiang, X., Zeng, H., Wang, Z., Zheng, J., *et al.* (2021) Reversible Hydrogenation of Ab2-Type Zr-Mg-Ni-V Based Hydrogen Storage Alloys. *Progress*

in Natural Science: *Materials International*, **31**, 319-323. https://doi.org/10.1016/j.pnsc.2021.01.008

[126] Erika, T., Joaquin, D., Ricardo, F., Fabricio, R., Fernando, Z. and Verónica, D. (2018) Molybdenum Incorporation on AB_2 Alloys-Part I Metallurgical and Electrochemical Characterization: Electrocatalytic Behavior. *Journal of Alloys and Compounds*, **744**, 583.

[127] Luo, L., Ye, X., Zhao, C., Zhang, G., Kou, H., Xiong, R., *et al.* (2020) Effects of Mo Substitution on the Kinetic and Thermodynamic Characteristics of $ZrCo_{1-x}Mo_x$ (x = 0-0.2) Alloys for Hydrogen Storage. *International Journal of Hydrogen Energy*, **45**, 2989-2998. https://doi.org/10.1016/j.ijhydene.2019.11.126

[128] Wu, T., Xue, X., Zhang, T., Hu, R., Kou, H. and Li, J. (2016) Role of Ni Addition on Hydrogen Storage Characteristics of ZrV2 Laves Phase Compounds. *International Journal of Hydrogen Energy*, **41**, 10391-10404. https://doi.org/10.1016/j.ijhydene.2014.10.023

[129] Tu, Y.L., Jiang, L.J., Guo, X.M., Jian, L., Zhao, W. and Wu, Y.F. (2014) Hydrogen Storage Properties of $ZrFe_{1.95-x}MnxV_{0.10}$ (x = 0, 0.05, 0.10, 0.15) Alloys. *Chinese Journal of Rare Metals*, **38**, 629.

[130] Ai, Y.C., Su, T., Huang, S.M., Xu, K. and Hou, X.L. (2022) Study on Zr-V-Fe-Cr Hydrogen Source for Lightweight Hydrogen Atomic Clock. *Astronomical Research & Technology*, **19**, 379.

[131] Qin, C., Wang, H., Jiang, W., Liu, J., Ouyang, L. and Zhu, M. (2022) Comparative Study of Ga and Al Alloying with $ZrFe_2$ for High-Pressure Hydrogen Storage. *International Journal of Hydrogen Energy*, **47**, 13409-13417. https://doi.org/10.1016/j.ijhydene.2021.12.110

[132] Yao, Z., Liang, Z., Xiao, X., Huang, X., Liu, J., Wang, X., *et al.* (2020) An Impact of Hydrogenation Phase Transformation Mechanism on the Cyclic Stabilizing Behavior of $Zr_{0.8}Ti_{0.2}Co$ Alloy for Hydrogen Isotope Handling. *Materials Today Energy*, **18**, Article ID: 100554. https://doi.org/10.1016/j.mtener.2020.100554

[133] Yao, Z., Liang, Z., Xiao, X., Qi, J., He, J., Huang, X., *et al.* (2022) Achieving Excellent Cycle Stability in Zr-Nb-Co-Ni Based Hydrogen Isotope Storage Alloys by Controllable Phase Transformation Reaction. *Renewable Energy*, **187**, 500-507. https://doi.org/10.1016/j.renene.2022.01.086

[134] Yu, Y.F., Ye, Y.M., Li, X.B., Kang, Y. and Hu, S.L. (2018) Study on Phase Structure and Hydrogen Absorption/Desorption Performance of ZrVFe Alloy. *Rare Metals and Cemented Carbides*, **46**, 49-53, 62.

[135] Wan, C., Jiang, X., Yin, X. and Ju, X. (2020) High-Capacity Zr-Based AB_2-Type Alloys as Metal Hydride Battery Anodes. *Journal of Alloys and Compounds*, **828**, Article ID: 154402. https://doi.org/10.1016/j.jallcom.2020.154402

[136] Lee, S., Kim, D., Yu, J., Jang, K. and Lee, J. (1998) The Effect of Annealing on the Discharge Characteristics of a Zr-V-Mn-Ni Hydrogen Storage Alloy. *Journal of The Electrochemical Society*, **145**, 1953-1957. https://doi.org/10.1149/1.1838581

[137] Zhang, Y., Li, J., Zhang, T., Wu, T., Kou, H. and Xue, X. (2017) Hydrogenation Thermokinetics and Activation Behavior of Non-Stoichiometric Zr-Based Laves Alloys with Enhanced Hydrogen Storage Capacity. *Journal of Alloys and Compounds*, **694**, 300-308. https://doi.org/10.1016/j.jallcom.2016.10.021

[138] Luo, Z., Leng, H., Han, X., Liu, W., Yang, G. and Ma, Z. (2022) Influence of Preparation Methods on the Hydrogen Absorption Properties of Zr_7V_5Fe Getter Alloy. *Journal of Alloys and Compounds*, **926**, Article ID: 166739. https://doi.org/10.1016/j.jallcom.2022.166739

[139] Wijayanti, I.D., Mølmen, L., Denys, R.V., Nei, J., Gorsse, S., Guzik, M.N., *et al.* (2019) Studies of Zr-Based C_{15} Type Metal Hydride Battery Anode Alloys Prepared by Rapid Solidification. *Journal of Alloys and Compounds*, **804**, 527-537. https://doi.org/10.1016/j.jallcom.2019.06.324

[140] Zhang, T., Zhang, Y., Zhang, M., Hu, R., Kou, H., Li, J., *et al.* (2016) Hydrogen Absorption Behavior of Zr-Based Getter Materials with Pd Ag Coating against Gaseous Impurities. *International Journal of Hydrogen Energy*, **41**, 14778-14787. https://doi.org/10.1016/j.ijhydene.2016.06.073

[141] Han, X., Yan, P., Zhang, D., Lv, L., Yang, G., Qin, L., *et al.* (2020) Hydrogen Absorption Behavior of Non-Stoichiometric $Zr_{7-x}Ti_xV_5Fe$ (x = 0, 0.3, 0.9, 1.5 and 2.1) Alloys. *International Journal of Hydrogen Energy*, **45**, 21625-21634. https://doi.org/10.1016/j.ijhydene.2020.05.194

[142] Cao, Z., Zhou, P., Xiao, X., Zhan, L., Jiang, Z., Wang, S., *et al.* (2022) Development of $Ti_{0.85}Zr_{0.17}$(Cr-Mn-V)$_{1.3}Fe_{0.7}$-Based Laves Phase Alloys for Thermal Hydrogen Compression at Mild Operating Temperatures. *Rare Metals*, **41**, 2588-2594. https://doi.org/10.1007/s12598-022-01962-x

[143] Yan, Y., Li, Z., Wu, Y. and Zhou, S. (2022) Hydrogen Absorption-Desorption Characteristic of $(Ti_{0.85}Zr_{0.15})_{1.1}Cr_1$-Xmoxmn Based Alloys with C_{14} Laves Phase. *Progress in Natural Science*: *Materials International*, **32**, 143-149. https://doi.org/10.1016/j.pnsc.2022.03.001

[144] Nygård, M.M., Sørby, M.H., Grimenes, A.A. and Hauback, B.C. (2020) The Influence of Fe on the Structure and Hydrogen Sorption Properties of Ti-V-Based Metal Hydrides. *Energies*, **13**, Article 2874. https://doi.org/10.3390/en13112874

[145] Pineda-Romero, N. and Zlotea, C. (2022) Uncovering the Effect of Al Addition on the Hydrogen Storage Properties of the Ternary TiVNb Alloy. *Materials*, **15**, Article 7974. https://doi.org/10.3390/ma15227974

[146] Zhou, P., Cao, Z., Xiao, X., Jiang, Z., Zhan, L., Li, Z., *et al.* (2022) Study on Low-Vanadium Ti-Zr-Mn-Cr-V Based Alloys for High-Density Hydrogen Storage. *International Journal of Hydrogen Energy*, **47**, 1710-1722. https://doi.org/10.1016/j.ijhydene.2021.10.106

[147] Tu, B., Wang, H., Wang, Y., Li, R., Ouyang, L. and Tang, R. (2022) Optimizing Ti-Zr-Cr-Mn-Ni-V Alloys for Hybrid Hydrogen Storage Tank of Fuel Cell Bicycle. *International Journal of Hydrogen Energy*, **47**, 14952-14960. https://doi.org/10.1016/j.ijhydene.2022.03.018

[148] Wijayanti, I.D., Denys, R., Suwarno, Volodin, A.A., Lototskyy, M.V., Guzik, M.N., *et al.* (2020) Hydrides of Laves Type Ti-Zr Alloys with Enhanced H Storage Capacity as Advanced Metal Hydride Battery Anodes. *Journal of Alloys and Compounds*, **828**, Article ID: 154354. https://doi.org/10.1016/j.jallcom.2020.154354

[149] Khajavi, S., Rajabi, M. and Huot, J. (2018) Crystal Structure of As-Cast and Heat-Treated $Ti_{0.5}Zr_{0.5}(Mn_{1-x}Fe_x)$ Cr_1, X=0, 0.2, 0.4. *Journal of Alloys and Compounds*, **767**, 432-438. https://doi.org/10.1016/j.jallcom.2018.07.111

[150] Stepanova, E., Pushilina, N., Syrtanov, M., Laptev, R. and Kashkarov, E. (2019) Hydrogen Effect on Ti-6.5Al-3.5Mo-1.5Zr-0.3Si Parts Produced by Electron Beam Melting. *International Journal of Hydrogen Energy*, **44**, 29380-29388. https://doi.org/10.1016/j.ijhydene.2019.03.156

[151] Khajavi, S., Rajabi, M. and Huot, J. (2019) Effect of Cold Rolling and Ball Milling on First Hydrogenation of $Ti_{0.5}Zr_{0.5}$ $(Mn_{1-X}Fe_x)$ Cr_1, X = 0, 0.2, 0.4. *Journal of Alloys and Compounds*, **775**, 912-920. https://doi.org/10.1016/j.jallcom.2018.10.179

[152] Liu, H., Tan, L., Guo, Y., Chen, P., Gao, S., Su, Z., *et al.* (2019) Fabrication and

Electrochemical Hydrogen Storage Performance of $Ti_{49}Zr_{26}Ni_{25}$ Alloy Covered with Cd/Pd Core/Shell Particles. *International Journal of Hydrogen Energy*, **44**, 24800-24809. https://doi.org/10.1016/j.ijhydene.2019.07.094

[153] Sujan, G.K., Pan, Z., Li, H., Liang, D. and Alam, N. (2019) An Overview on TiFe Intermetallic for Solid-State Hydrogen Storage: Microstructure, Hydrogenation and Fabrication Processes. *Critical Reviews in Solid State and Materials Sciences*, **45**, 410-427. https://doi.org/10.1080/10408436.2019.1652143

[154] Lv, P. and Huot, J. (2016) Hydrogen Storage Properties of $Ti_{0.95}FeZr_{0.05}$, $TiFe_{0.95}Zr_{0.05}$ and $TiFeZr_{0.05}$ Alloys. *International Journal of Hydrogen Energy*, **41**, 22128-22133. https://doi.org/10.1016/j.ijhydene.2016.07.091

[155] Lin, J. (2018) Preparation and Electrochemical Hydrogen Storage Properties of TiVNi Composites. *Jilin University*, No. 12, 119.

[156] Zhai, T., Wei, Z., Yuan, Z., Han, Z., Feng, D., Wang, H., *et al.* (2021) Influences of La Addition on the Hydrogen Storage Performances of TiFe-Base Alloy. *Journal of Physics and Chemistry of Solids*, **157**, Article ID: 110176. https://doi.org/10.1016/j.jpcs.2021.110176

[157] Liu, F.C., Han, Z.G., Yuan, Z.M., Zhai, T.T., Feng, D.C. and Zhang, Y.H. (2022) Effect of La Substitution for Ti on the Microstructure and Electrochemical Properties of TiFe Hydrogen Storage Alloys. *Metallic Functional Materials*, **29**, 90.

[158] Han, Z., Yuan, Z., Zhai, T., Feng, D., Sun, H. and Zhang, Y. (2023) Effect of Yttrium Content on Microstructure and Hydrogen Storage Properties of TiFe-Based Alloy. *International Journal of Hydrogen Energy*, **48**, 676-695. https://doi.org/10.1016/j.ijhydene.2022.09.227

[159] Zhang, Y., Shang, H., Gao, J., Zhang, W., Wei, X. and Yuan, Z. (2021) Effect of Sm Content on Activation Capability and Hydrogen Storage Performances of TiFe Alloy. *International Journal of Hydrogen Energy*, **46**, 24517-24530. https://doi.org/10.1016/j.ijhydene.2021.05.017

[160] Xu, Q.F., Zhai, T.T., Han, Z.G. and Zhang, Y.H. (2021) Effect of Pr Substitution of Ti on Microstructure and Electrochemical Properties of TiFe Based Hydrogen Storage Alloy. *Metallic Functional Materials*, **28**, 42.

[161] Shang, H., Zhang, Y., Li, Y., Gao, J., Zhang, W., Wei, X., *et al.* (2022) Effect of Pr Content on Activation Capability and Hydrogen Storage Performances of TiFe Alloy. *Journal of Alloys and Compounds*, **890**, Article ID: 161785. https://doi.org/10.1016/j.jallcom.2021.161785

[162] Lee, S., Ha, T., Lee, Y., Kim, D., Suh, J., Cho, Y.W., *et al.* (2021) EBSD Microstructural Analysis of AB-Type TiFe Hydrogen Storage Alloys. *Materials Characterization*, **178**, Article ID: 111276. https://doi.org/10.1016/j.matchar.2021.111276

[163] Li, Y., Shang, H., Zhang, Y., Li, P., Qi, Y. and Zhao, D. (2019) Investigations on Gaseous Hydrogen Storage Performances and Reactivation Ability of As-Cast $TiFe_1$-Ni (x=0, 0.1, 0.2 and 0.4) Alloys. *International Journal of Hydrogen Energy*, **44**, 4240-4252. https://doi.org/10.1016/j.ijhydene.2018.12.144

[164] Dematteis, E.M., Dreistadt, D.M., Capurso, G., Jepsen, J., Cuevas, F. and Latroche, M. (2021) Fundamental Hydrogen Storage Properties of TiFe-Alloy with Partial Substitution of Fe by Ti and Mn. *Journal of Alloys and Compounds*, **874**, Article ID: 159925. https://doi.org/10.1016/j.jallcom.2021.159925

[165] Dematteis, E.M., Cuevas, F. and Latroche, M. (2021) Hydrogen Storage Properties of Mn and Cu for Fe Substitution in $TiFe_{0.9}$ Intermetallic Compound. *Journal of Alloys and Compounds*, **851**, Article ID: 156075. https://doi.org/10.1016/j.jallcom.2020.156075

[166] Ali, W., Hao, Z., Li, Z., Chen, G., Wu, Z., Lu, X., *et al.* (2017) Effects of Cu and Y Substitution on Hydrogen Storage Performance of $TiFe_{0.86}Mn_{0.1}Y_{0.1-x}Cu_x$. *International Journal of Hydrogen Energy*, **42**, 16620-16631. https://doi.org/10.1016/j.ijhydene.2017.04.247

[167] Li, C., Gao, X., Liu, B., Wei, X., Zhang, W., Lan, Y., *et al.* (2023) Effects of Zr Doping on Activation Capability and Hydrogen Storage Performances of TiFe-Based Alloy. *International Journal of Hydrogen Energy*, **48**, 2256-2270. https://doi.org/10.1016/j.ijhydene.2022.10.098

[168] Faisal, M., Kim, J., Cho, Y.W., Jang, J., Suh, J., Shim, J., *et al.* (2021) Design of V-Substituted TiFe-Based Alloy for Target Pressure Range and Easy Activation. *Materials*, **14**, Article 4829. https://doi.org/10.3390/ma14174829

[169] Leng, H., Yu, Z., Luo, Q., Yin, J., Miao, N., Li, Q., *et al.* (2020) Effect of Cobalt on the Microstructure and Hydrogen Sorption Performances of $TiFe_{0.8}Mn_{0.2}$ Alloy. *International Journal of Hydrogen Energy*, **45**, 19553-19560. https://doi.org/10.1016/j.ijhydene.2020.05.130

[170] Shang, H., Zhang, Y., Li, Y., Qi, Y., Guo, S. and Zhao, D. (2019) Effects of Adding Over-Stoichiometrical Ti and Substituting Fe with Mn Partly on Structure and Hydrogen Storage Performances of TiFe Alloy. *Renewable Energy*, **135**, 1481-1498. https://doi.org/10.1016/j.renene.2018.09.072

[171] Liu, H., Zhang, J., Sun, P., Zhou, C., Liu, Y. and Fang, Z.Z. (2023) Effect of Oxygen Addition on Phase Composition and Activation Properties of TiFe Alloy. *International Journal of Hydrogen Energy*, **48**, 8563-8572. https://doi.org/10.1016/j.ijhydene.2022.11.353

[172] Alam, M.M., Sharma, P. and Huot, J. (2018) Effect of Addition of Lanthanum on the Hydrogen Storage Properties of TiFe Alloy. *Acta Crystallographica Section A Foundations and Advances*, **74**, a146. https://doi.org/10.1107/s0108767318098537

[173] Lv, P. and Huot, J. (2017) Hydrogenation Improvement of TiFe by Adding $ZrMn_2$. *Energy*, **138**, 375-382. https://doi.org/10.1016/j.energy.2017.07.072

[174] Patel, A.K., Duguay, A., Tougas, B., Schade, C., Sharma, P. and Huot, J. (2020) Microstructure and First Hydrogenation Properties of TiFe Alloy with Zr and Mn as Additives. *International Journal of Hydrogen Energy*, **45**, 787-797. https://doi.org/10.1016/j.ijhydene.2019.10.239

[175] Patel, A., Duguay, A., Tougas, B., Neumann, B., Schade, C., Sharma, P., *et al.* (2021) Study of the Microstructural and First Hydrogenation Properties of TiFe Alloy with Zr, Mn and V as Additives. *Processes*, **9**, Article 1217. https://doi.org/10.3390/pr9071217

[176] Shang, H., Zhang, Y., Gao, J., Zhang, W., Wei, X., Yuan, Z., *et al.* (2022) Characteristics of Electrochemical Hydrogen Storage Using Ti-Fe Based Alloys Prepared by Ball Milling. *International Journal of Hydrogen Energy*, **47**, 1036-1047. https://doi.org/10.1016/j.ijhydene.2021.10.068

[177] Li, Y., Zhang, Y., Shang, H., Gao, J., Zhang, W. and Ju, L. (2023) Hydrogen Storage Characteristics of $Ti_{1.04}Fe_{0.7}Ni_{0.1}Zr_{0.1}Mn_{0.1}Pr_{0.06}$ Alloy Treated by Ball Milling. *Journal of Alloys and Compounds*, **930**, Article ID: 167024. https://doi.org/10.1016/j.jallcom.2022.167024

[178] Yuan, Z., Sui, Y., Yuan, Q., Qi, Z., Zhai, T., Li, X., *et al.* (2023) Effects of Ball Milling Time on the Microstructure and Hydrogen Storage Performances of $Ti_{21.7}Y_{0.3}Fe_{16}Mn_3Cr$ Alloy. *International Journal of Hydrogen Energy*, **48**, 11340-11351. https://doi.org/10.1016/j.ijhydene.2022.09.027

[179] Ha, T., Lee, S., Hong, J., Lee, Y., Kim, D., Suh, J., *et al.* (2021) Hydrogen Storage

Behavior and Microstructural Feature of a TiFe-$ZrCr_2$ Alloy. *Journal of Alloys and Compounds*, **853**, Article ID: 157099. https://doi.org/10.1016/j.jallcom.2020.157099

[180] Pei, P., Zhang, P.L., Zhang, B. and Song, X.P. (2006) V Based Hydrogen Storage Alloys and Alloying Research. *Materials Reports*, No. 10, 123.

[181] Hang, Z.M., Bin, Z.G., Xu, H. and Wen, W.X. (2014) Microstructure and Electrochemical Properties of $Ti_{0.4}Zr_{0.1}V_{1.1}Mn_{0.5}Ni_{0.4}Crx$ (x = 0, 0.1, 0.2, 0.3) Alloys. *Journal of Material Sciences & Engineering*, **32**, 52.

[182] Chen, X.Y., Chen, R.R., Yu, K., Ding, X., Li, X.Z., Ding, H.S., *et al.* (2019) Effect of Ce Substitution on Hydrogen Absorption/Desorption of Laves Phase-Related BCC Solid Solution $Ti_{33}V_{37}Mn_{30}$ Alloy. *Journal of Alloys and Compounds*, **783**, 617-624. https://doi.org/10.1016/j.jallcom.2018.12.302

[183] Xue, X., Ma, C., Liu, Y., Wang, H. and Chen, Q. (2023) Impacts of Ce Dopants on the Hydrogen Storage Performance of Ti-Cr-V Alloys. *Journal of Alloys and Compounds*, **934**, Article ID: 167947. https://doi.org/10.1016/j.jallcom.2022.167947

[184] Tong, Y.W., Li, N.L. and Zhang, X.F. (2021) Effect of Addition Amount of Rare Rarth Ce on Micro-Structure and Electrochemical Properties of V-Based Hydrogen Storage Alloys. *Rare Metals and Cemented Carbides*, **49**, 42.

[185] Kong, L., Li, X., Young, K., Nei, J., Liao, X. and Li, W. (2018) Effects of Rare-Earth Element Additions to Laves Phase-Related Body-Centered-Cubic Solid Solution Metal Hydride Alloys: Thermodynamic and Electrochemical Properties. *Journal of Alloys and Compounds*, **737**, 174-183. https://doi.org/10.1016/j.jallcom.2017.12.058

[186] Luo, L., Li, Y., Yuan, Z., Liu, S., Singh, A., Yang, F., *et al.* (2022) Nanoscale Microstructures and Novel Hydrogen Storage Performance of as Cast $V_{47}Fe_{11}Ti_{30}Cr_{10}RE_2$ (RE = La, Ce, Y, Sc) Medium Entropy Alloys. *Journal of Alloys and Compounds*, **913**, Article ID: 165273. https://doi.org/10.1016/j.jallcom.2022.165273

[187] Luo, L., Li, Y., Zhai, T., Hu, F., Zhao, Z., Bian, X., *et al.* (2019) Microstructure and Hydrogen Storage Properties of $V_{48}Fe_{12}Ti_{15}$-$Cr_{25}Al$ (x=0, 1) Alloys. *International Journal of Hydrogen Energy*, **44**, 25188-25198. https://doi.org/10.1016/j.ijhydene.2019.02.172

[188] Chanchetti, L.F., Hessel Silva, B., Montero, J., Zlotea, C., Champion, Y., Botta, W.J., *et al.* (2023) Structural Characterization and Hydrogen Storage Properties of the $Ti_{31}V_{26}Nb_{26}Zr_{12}M_5$ (M = Fe, Co, or Ni) Multi-Phase Multicomponent Alloys. *International Journal of Hydrogen Energy*, **48**, 2247-2255. https://doi.org/10.1016/j.ijhydene.2022.10.060

[189] Hang, Z., Chen, L., Xiao, X., Yao, Z., Shi, L., Feng, Y., *et al.* (2021) Microstructure and Hydrogen Storage Properties of $Ti_{10+x}V_{80-x}Fe_6Zr_4$ (x = 0~15) Alloys. *International Journal of Hydrogen Energy*, **46**, 27622-27630. https://doi.org/10.1016/j.ijhydene.2021.06.019

[190] Balcerzak, M., Wagstaffe, M., Robles, R., Pruneda, M. and Noei, H. (2020) Effect of Cr on the Hydrogen Storage and Electronic Properties of BCC Alloys: Experimental and First-Principles Study. *International Journal of Hydrogen Energy*, **45**, 28996-29008. https://doi.org/10.1016/j.ijhydene.2020.07.186

[191] Hang, Z.M., Xiao, X., Wen, W.X., Bin, Z.G., Huang, S.M., Xu, H. and Chen, L.X. (2016) Influence of Partial Substitution of Zr for Ti in Low-Vanadium Alloy $Ti_{20}Cr_{24}Mn_8V_{40}Fe_8$ on Its Micro-Structure and Hydrogen Storage Properties. *Journal of Materials Science*, **34**, 874.

[192] Mao, Y., Yang, S., Wu, C., Luo, L. and Chen, Y. (2017) Preparation of $(FeV_{80})_{48}Ti_{26+x}Cr_{26}$ (x = 0 – 4) Alloys by the Hydride Sintering Method and Their

Hydrogen Storage Performance. *Journal of Alloys and Compounds*, **705**, 533-538. https://doi.org/10.1016/j.jallcom.2017.02.166

[193] Chen, X.Y., Liu, B., Zhang, S.B., Ding, X. and Chen, R.R. (2022) Effect of Heat Treatment on Microstructure and Thermal Stability of $Ti_{19}Hf_4V_{40}Mn_{35}Cr_2$ Hydrogen Storage Alloy. *Journal of Alloys and Compounds*, **917**, Article ID: 165355. https://doi.org/10.1016/j.jallcom.2022.165355

[194] Liu, B., Chen, X., Zhang, S., Ding, X. and Chen, R. (2023) Formation of Eutectic and Hydrogen Absorption/Desorption Behavior of Heat-Treated $Ti_{19}Hf_4V_{40}Mn_{35}Cr_2$ Alloys. *Intermetallics*, **152**, Article ID: 107752. https://doi.org/10.1016/j.intermet.2022.107752

[195] Chen, Z., Luo, L., Su, Z., Liu, W., Zhang, F. and Huang, Y. (2019) Effect of LaH_3 Additive on Microstructures and Hydrogen Storage Properties of $V_{40}Ti_{26}Cr_{26}Fe_8$ Alloys Prepared by Hydride Powder Sintering Method. *International Journal of Hydrogen Energy*, **44**, 13538-13548. https://doi.org/10.1016/j.ijhydene.2019.03.038

[196] Silva, B.H., Zlotea, C., Vaughan, G., Champion, Y., Botta, W.J. and Zepon, G. (2022) Hydrogen Absorption/Desorption Reactions of the $(TiVNb)_{85}Cr_{15}$ Multicomponent Alloy. *Journal of Alloys and Compounds*, **901**, Article ID: 163620. https://doi.org/10.1016/j.jallcom.2022.163620

[197] Han, Y., Wu, C., Wang, Q., Sun, D., Cheng, W., Li, X., *et al.* (2022) Phase Evolution Process and Hydrogen Storage Performances of $V_{72}Ti_{18}Cr_{10}$ Alloy Prepared by Co-Precipitation-Reduction Method. *Progress in Natural Science: Materials International*, **32**, 407-414. https://doi.org/10.1016/j.pnsc.2022.06.002

[198] Zhang, J., Li, P., Huang, G., Zhang, W., Hu, J., Xiao, H., *et al.* (2021) Superior Hydrogen Sorption Kinetics of $Ti_{0.20}Zr_{0.20}Hf_{0.20}Nb_{0.40}$ High-Entropy Alloy. *Metals*, **11**, Article 470. https://doi.org/10.3390/met11030470

[199] Shen, B.Z., Fan, J.F. and Guo, H.J. (2021) Study of the Hydrogen Storage Properties of Magnesium-Containing Mg_xTiVNiAlCr High Entropy Alloy. *Foundry Technology*, **42**, 565.

[200] Jiao, W.N., Lu, Y.P., Cao, Z.Q., Wang, T.M., Li, Y.J. and Yin, G.M. (2022) Progress and Prospect of Eutectic High Entropy Alloys. *Special Casting & Nonferrous Alloys*, **42**, 265.

[201] Sun, Y.H., Han, L.N., Gao, R.Y. and Xiong, Z.P. (2022) Research Progress of As-Cast Eutectic High-Entropy Alloys. *Nonferrous Metals Science and Engineering*, **13**, 27.

[202] Luo, L., Chen, L.P., Li L.R., *et al.* (2023) High-Entropy Alloys for Solid Hydrogen Storage: A Review. *International Journal of Hydrogen Energy*, **50**, 404-430. https://doi.org/10.1016/j.ijhydene.2023.07.146

[203] Cheng, B., Li, Y.K., Li, X.X., Ke, H.B., *et al.* (2023) Solid-State Hydrogen Storage Properties of Ti-V-Nb-Cr High-Entropy Alloys and the Associated Effects of Transitional Metals (M = Mn, Fe, Ni). *Acta Metallurgica Sinica-English Letters*, **36**, 1113-1122. https://doi.org/10.1007/s40195-022-01403-9

[204] Yang, F., Wang, J., Zhang, Y., Wu, Z., Zhang, Z., Zhao, F., *et al.* (2022) Recent Progress on the Development of High Entropy Alloys (HEAs) for Solid Hydrogen Storage: A Review. *International Journal of Hydrogen Energy*, **47**, 11236-11249. https://doi.org/10.1016/j.ijhydene.2022.01.141

[205] Sahlberg, M., Karlsson, D., Zlotea, C. and Jansson, U. (2016) Superior Hydrogen Storage in High Entropy Alloys. *Scientific Reports*, **6**, Article No. 36770. https://doi.org/10.1038/srep36770

[206] Chen, J., Li, Z., Huang, H., Lv, Y., Liu, B., Li, Y., *et al.* (2022) Superior Cycle Life of

Tizrfemncrv High Entropy Alloy for Hydrogen Storage. *Scripta Materialia*, **212**, Article ID: 114548. https://doi.org/10.1016/j.scriptamat.2022.114548

[207] Park, K.B., Park, J., Kim, Y.D., Fadonougbo, J.O., Kim, S., Kim, H., *et al.* (2021) Characterizations of Hydrogen Absorption and Surface Properties of $Ti_{0.2}Zr_{0.2}Nb_{0.2}V_{0.2}Cr_{0.17}Fe_{0.03}$ High Entropy Alloy with Dual Phases. *Metals and Materials International*, **28**, 565-571. https://doi.org/10.1007/s12540-021-01071-x

[208] Edalati, P., Floriano, R., Mohammadi, A., Li, Y., Zepon, G., Li, H., *et al.* (2020) Reversible Room Temperature Hydrogen Storage in High-Entropy Alloy TiZrCrMnFeNi. *Scripta Materialia*, **178**, 387-390. https://doi.org/10.1016/j.scriptamat.2019.12.009

[209] Zhang, C., Song, A., Yuan, Y., Wu, Y., Zhang, P., Lu, Z., *et al.* (2020) Study on the Hydrogen Storage Properties of a TiZrNbTa High Entropy Alloy. *International Journal of Hydrogen Energy*, **45**, 5367-5374. https://doi.org/10.1016/j.ijhydene.2019.05.214

[210] Fukagawa, T., Saito, Y. and Matsuyama, A. (2022) Effect of Varying Ni Content on Hydrogen Absorption-Desorption and Electrochemical Properties of Zr-Ti-Ni-Cr-Mn High-Entropy Alloys. *Journal of Alloys and Compounds*, **896**, Article ID: 163118. https://doi.org/10.1016/j.jallcom.2021.163118

[211] Ma, X., Ding, X., Chen, R., Gao, X., Su, Y. and Cui, H. (2022) Enhanced Hydrogen Storage Properties of $ZrTiVAL_{1-x}Fe_x$ High-Entropy Alloys by Modifying the Fe Content. *RSC Advances*, **12**, 11272-11281. https://doi.org/10.1039/d2ra01064j

[212] Floriano, R., Zepon, G., Edalati, K., Fontana, G.L.B.G., Mohammadi, A., Ma, Z., *et al.* (2020) Hydrogen Storage in Tizrnbfeni High Entropy Alloys, Designed by Thermodynamic Calculations. *International Journal of Hydrogen Energy*, **45**, 33759-33770. https://doi.org/10.1016/j.ijhydene.2020.09.047